

TOPICAL REVIEW

Review of Reduced Switch-Count Power Cells for Regenerative Cascaded H-Bridge Motor Drives

DOHO KANG^{1,2}, SARAH BADAWI^{1,3}, (Graduate Student Member, IEEE),
ZHITUO NI², (Member, IEEE), AHMED H. ABUELNAGA^{2,3}, (Member, IEEE),
MEHDI NARIMANI¹, (Senior Member, IEEE), AND NAVID R. ZARGARI^{1,2}, (Fellow, IEEE)

¹Electrical and Computer Engineering Department, McMaster University, Hamilton, ON L8S 4L8, Canada

²Rockwell Automation Inc., Cambridge, ON N1R 5N9, Canada

³Electrical Power and Machines Engineering Department, Ain Shams University, Cairo 11535, Egypt

Corresponding author: Sarah Badawi (badaws1@mcmaster.ca)

This work was supported in part by Rockwell Automation, Canada, and in part by the Natural Sciences and Engineering Research Council of Canada (NSERC).

ABSTRACT Cascaded H-Bridge (CHB) topology is one of the attractive topologies in high-power medium-voltage motor drive applications due to its modularity and scalability. Research in high power regenerative motor drives has gained significant attention with the increasing demand for efficient energy use. In a cascaded H-Bridge (CHB) converter, the regenerative capability can be introduced by replacing diode front end (DFE) with active front end (AFE) topologies. However, this results in a huge increase in the number of power semiconductors, gate drivers, and heat sink size and thus increases the overall size and cost of the regenerative CHB motor drives. To overcome the aforementioned challenges, different power cell designs have been introduced to reduce the switch count, allowing the design of more suitable-sized and more economical drives. This paper comprehensively reviews the reduced switch-count power cell designs, including single-phase and three-phase grid connections. Each reduced switch-count cell design is analyzed, and its advantages and disadvantages are studied in detail. The challenges that arise with each design and the method to address the challenges are discussed.

INDEX TERMS Cascaded H-bridge (CHB), reduced switch-count, control, motor drives, active front end, multilevel converter.


I. INTRODUCTION

Multilevel inverters (MLI) have been a core component in medium-voltage (MV) and high-voltage power converters due to their modularity, scalability, fault-tolerance capability, and the use of low voltage devices in high power applications [1]–[14]. These MLIs can be found widely in different applications, such as medium voltage motor drives [14]–[16], renewable energy generation [17]–[19], High Voltage Direct Current (HVDC) transmission systems [20], [21].

MLIs can be classified into two main categories: MLIs with single DC source and with multiple DC sources. Fig. 1 shows the various MLIs under the two groups [22]–[25]. The Cascaded H-Bridge (CHB), Neutral Point Clamped (NPC) converter, and Flying Capacitor (FC) converter, shown in

Fig. 2, are the basic and most notable voltage-source MLIs [22]–[24]. CHB MLI was first introduced in [26], where separate and isolated DC sources are used by multiple single-phase inverters connected in cascade to synthesize the multilevel waveform. In [27]–[29], the structure and control of NPC MLI were presented where a single DC-source can be used, however, it requires the use of high number of clamping diodes. Modified MLIs based on NPC topology were introduced after that [30]–[36]. The FC MLI was introduced in [37] and [38] with one DC source and multiple flying capacitors.

In MV motor drives, many manufacturers have used these three converters in their field applications [39]–[58], with different power ratings, front-end designs, cooling systems, control approaches, and other technical specifications as shown in Table 1 [6], [14]. From the table, it can be seen that CHB MLIs are widely used in applications with voltages

The associate editor coordinating the review of this manuscript and approving it for publication was Feifei Bu .

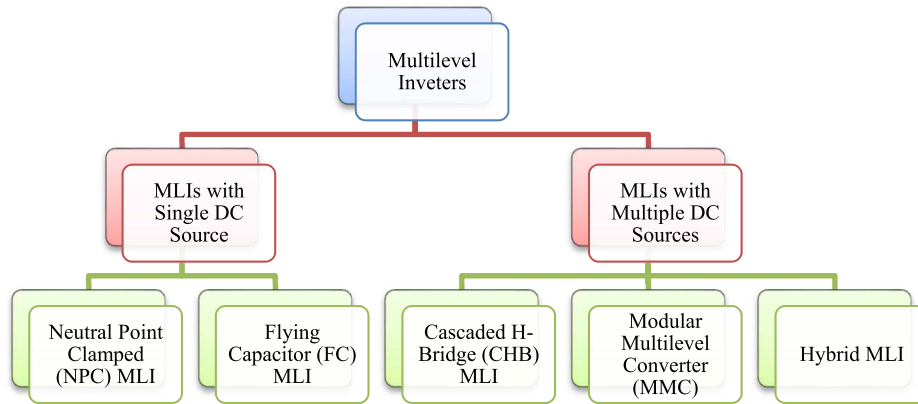


FIGURE 1. Multilevel inverters classification.

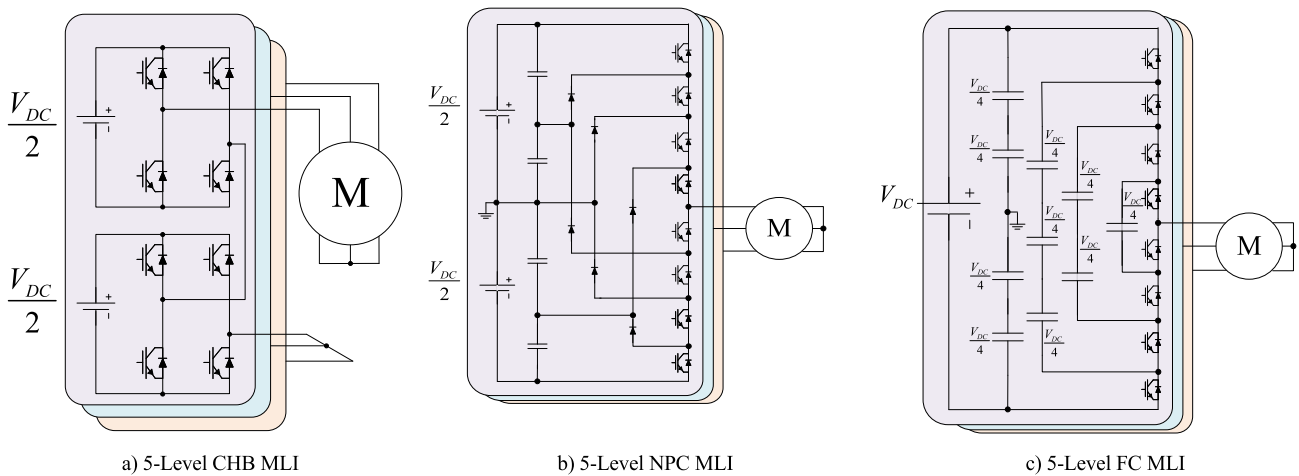


FIGURE 2. Basic MLI topologies (CHB, NPC, and FC).

TABLE 1. Number of components to produce m voltage levels [6], [14].

Parameters	Multilevel Converter		
	3L-NPC [39]–[44], [46], [47], [52]	CHB [40], [41], [45], [48]–[51], [55]–[58]	4L-FC[53]
Max. Power	27MW, 31.5MVA, 40MVA, 44MW, 33.6MW, 3.7MW, 27MVA, 10MW	120MW, 15MW, 5.6MW, 10MVA, 11.1MVA, 6MVA, 6.25MVA, 16.7MVA, 24.4MVA	2.24
Output Voltage [kV]	2.3/3.3/4.0/4.16/6.6	2.3/3/3.3/4.16/6/6.6/10/11	2.3/3.3/4.16
Max Output Frequency [Hz]	82.5, 250, 90, 140, 300, 120, 100	330, 120-,	120
Diode Front End (no. of pulses)	12/18/24/36	18/24/30/42/48/54	18/24/36
Active Front End option	3L-NPC back-to-back	2L-VSI per cell	4L-FC back-to-back
Modulation Method	PWM, SHE, SVM	PS-PWM	PS-PWM
No. of Voltage Levels	3	7/11/13/15/17/19	4
No. of Power Cells	1	3/4/5/6/7/8/9	3

higher than 6.6 kV and high number of voltage levels. This is due to the several advantages of CHB MLIs. As shown in Table 2 [59], the CHB topology uses the least number of

components to produce the same number of voltage levels as the other two topologies. Based on the output requirement of the system, a power cell can be added or removed without

TABLE 2. Number of components to produce m voltage levels [59].

Topology	CHB	NPC	FC
Main Switching Devices	$2(m-1)$	$2(m-1)$	$2(m-1)$
Clamping Diodes	0	$(m-1)(m-2)$	0
DC-link Capacitors	$(m-1)/2$	$(m-1)$	$(m-1)$
Flying Capacitors	0	1	$(m-1)(m-2)/2$

impacting the performance of the other power cells in the system [14]. The modular structure of the CHB provides a single design that can accommodate different power ratings based on the number of power cells.

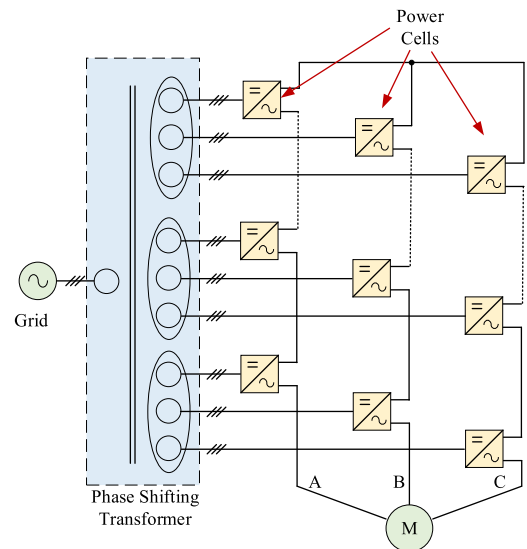
TABLE 3. Regenerative applications [60].

Industry Segment	Applications
Cement	<ul style="list-style-type: none"> Material handling conveyors Pre-heater induced draft fans Ball mills
Marine (Commercial)	<ul style="list-style-type: none"> Propulsion and positioning drives Anchor handling
Mining	<ul style="list-style-type: none"> Bucket wheel excavator and reclaimer Dragline
Oil and Gas	<ul style="list-style-type: none"> Drill stem Oil centrifuge Pipeline booster pump
Power Generation	<ul style="list-style-type: none"> Boiler induced draft fan

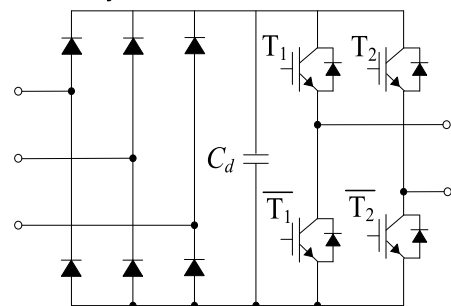
The conventional CHB motor drive is shown in Fig.3, each power cell is equipped with a six-pulse diode rectifier, shown in Fig. 3(a), that converts the input three-phase AC voltages to DC voltage used by the output H-bridge inverter. However, using a six-pulse diode rectifier introduces low-order harmonics on the primary current. A phase-shifting transformer is employed to apply the appropriate phase shift on the secondary side of the transformer to cancel the low-order harmonics and provide isolated dc to each power cell.

The uncontrolled diode rectifier allows only the unidirectional power flow from the grid to the load. However, there are several applications such as downhill conveyors, cranes, and hoists, or where the load can overhaul the motor and the rated power can be regenerated from the motor side [60]. Table 3 shows some of these regenerative applications.

In conventional CHB motor drives with diode front end (DFE) configuration, this regenerated energy is dissipated, making the system energy-inefficient [60]. If the power cell does not have any devices where the energy can be dissipated,



a) CHB Motor Drive System



b) Conventional Power Cell

FIGURE 3. A typical n-cell CHB motor drive.

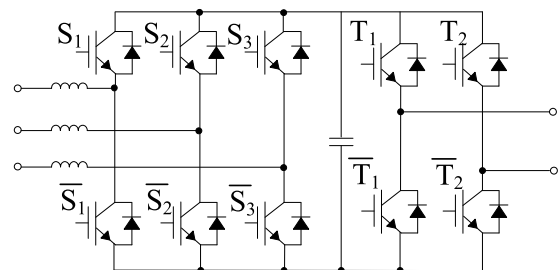


FIGURE 4. Regenerative power cell.

this can cause the DC link voltage to increase. A braking resistor or a chopper circuit, seen in [61], can be used to dissipate the excess energy in the power cell safely. However,

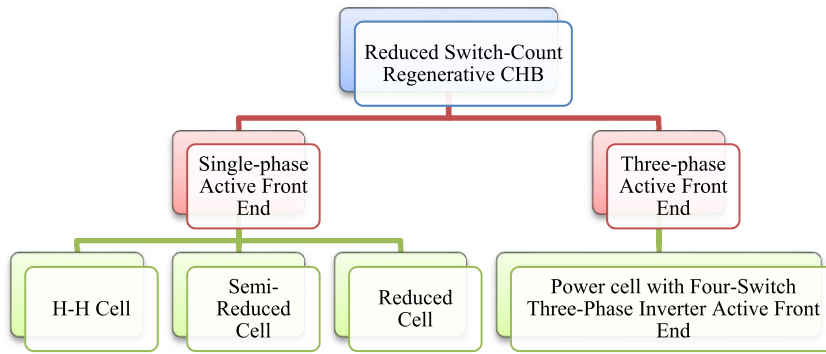


FIGURE 5. Classification of reduced switch-count regenerative CHB power cells.

using a resistor will mean that the energy is lost as heat and a chopper circuit introduces additional devices and complexity to the system.

A regenerative power cell topology has been proposed to address the energy loss and improve the characteristics of the CHB. In the regenerative power cell topology, diodes are replaced with IGBT switches to allow bi-directional current flow with the grid, allowing control over the active and reactive power used by the CHB inverter. The regenerative power cell in [62] and [63] can be seen in Fig. 4.

However, using a regenerative power cell as a replacement for a traditional DFE power cell proposes a significant increase in the number of switches required as six diodes are replaced with six IGBT switches. The replacement ultimately leads to a larger footprint, more advanced heatsink design, and higher cost.

The research in switch-count reduction has been an attractive area to reduce the total number of switches required per power cell with many feasible options such as the H-H cell, Semi-Reduced Cell, Reduced cell, and Three-Phase Reduced Switch-Count cell as shown in Fig. 5 [64]–[69].

In this paper, a review of each existing reduced switch-count cell is conducted, emphasizing the characteristics and challenges of each cell. Each cell is compared with the conventional regenerative power cell, as seen in Fig. 2.

A reduced switch-count regenerative power cell that aims to replace the conventional regenerative power cell has aspects that should be considered to ensure a successful design [64], [66]–[68]:

- 1) Power cell structure
- 2) Ease and simplicity of active front end (AFE) control scheme implementation
- 3) DC-link voltage ripples
- 4) Compliance with the grid connection standards
- 5) Good dynamic performance
- 6) Stability against grid side disturbances
- 7) Reactive power compensation capability
- 8) Switches current and voltage ratings

This paper evaluates three single-phase reduced switch-count regenerative CHB power cells and one three-phase reduced switch-count regenerative CHB power cell in terms of structure, control, and switches ratings. The benchmark for

comparison is the conventional regenerative CHB power cell shown in Fig. 4.

The paper is organized as follows: the conventional regenerative CHB power cell operation and control is discussed in section II. In section III, the three single-phase reduced switch-count regenerative power cells are reviewed. The three-phase reduced switch-count regenerative power cell is reviewed in section IV. Different design aspects are discussed in section V, while comparison between the different reduced switch-count power cells and the conventional regenerative power cell is shown in section VI. Future trends and conclusions are drawn in sections VII and VIII.

II. CONVENTIONAL REGENERATIVE POWER CELL

Fig. 4 shows the conventional regenerative CHB power cell introduced in [62] and [63]. A 2L-VSI replaces the three-phase uncontrolled rectifier, and the front end is controlled by PWM technique. The controlled front end allows bidirectional power flow and can compensate reactive power.

Due to the absence of low order harmonics, the conventional phase-shifting transformer can be replaced by a simpler multi-winding transformer since the low order harmonics do not exist any longer.

The typical AFE control block diagram is shown in Fig. 6 and is based on the Voltage-Oriented Control (VOC) scheme. It has two control loops. [63]. The DC-link voltage is regulated by the DC-link voltage controller in order to be equal to the reference value. The output of the DC-link controller is the value and direction of the required active power, while the reactive power is directly controlled to the desired value and is usually set to zero for unity power factor. Both reference values are used as the input to the current control loop which is based on the system d - q power equations [63]:

$$\begin{aligned} P &= \frac{3}{2}(v_d i_d + v_q i_q) \\ Q &= \frac{3}{2}(v_q i_d - v_d i_q), \end{aligned} \quad (1)$$

where v_d , v_q , i_d , and i_q are the d and q components of the grid voltage, the cell input current respectively.

To get the d - q components, the abc -to- dq transformation in (2) is applied to the measured grid voltages and cell input currents. v_d is made aligned with the grid voltage through

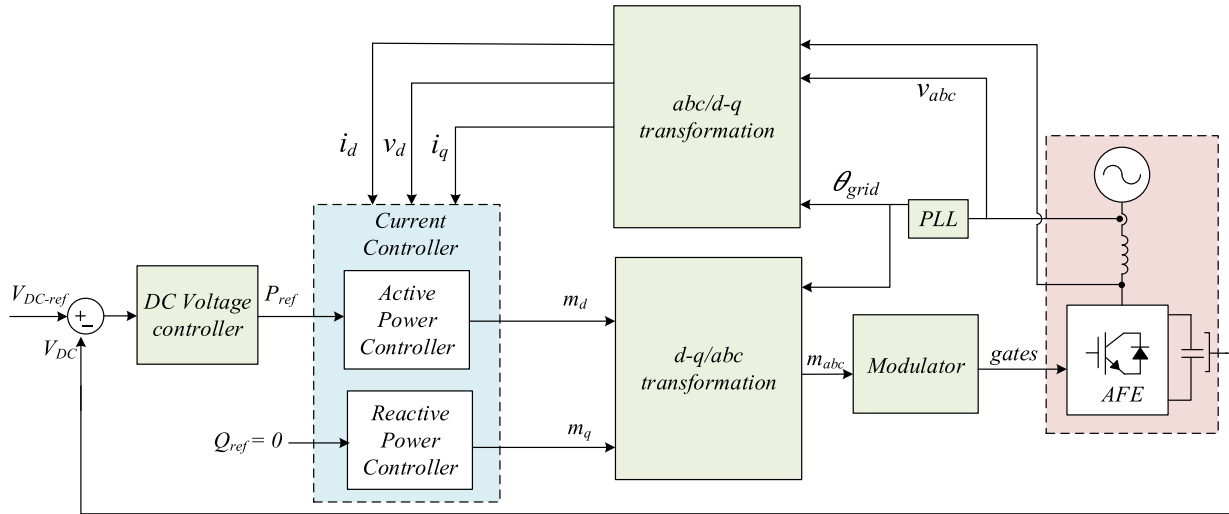


FIGURE 6. Conventional regenerative power cell active front end control scheme [63].

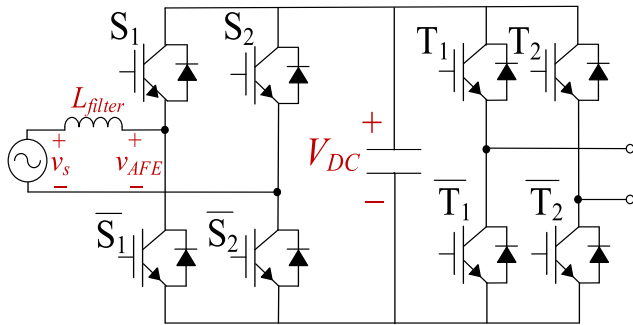


FIGURE 7. H-H Cell proposed in [10].

using the grid voltage angle as the angle of the transformation (θ), this way v_q is set to zero. To estimate the grid voltage angle, a phase-locked loop (PLL) is needed in the system [63].

$$\begin{bmatrix} x_d \\ x_q \\ x_0 \end{bmatrix} = \frac{2}{3} \begin{bmatrix} \cos(\theta) & \cos\left(\theta - \frac{2\pi}{3}\right) & \cos\left(\theta + \frac{2\pi}{3}\right) \\ -\sin(\theta) & -\sin\left(\theta - \frac{2\pi}{3}\right) & -\sin\left(\theta + \frac{2\pi}{3}\right) \\ \frac{1}{2} & \frac{1}{2} & \frac{1}{2} \end{bmatrix} \times \begin{bmatrix} x_a \\ x_b \\ x_c \end{bmatrix} \quad (2)$$

As the conventional regenerative CHB power cell has a 2L-VSI front end, the DC-link is subjected to high switching frequency ripples. In addition to this, it is subjected to second order harmonic ripples of the output frequency from the H-bridge inverter side [62], [63].

Although the conventional regenerative power cell offers bidirectional power flow capability, the high number of switches in the cell - 10 switches - leads to high cost and high switching power losses.

III. REVIEW OF SINGLE-PHASE REDUCED SWITCH-COUNT POWER CELLS

A. H-H POWER CELL

1) POWER CELL STRUCTURE

As seen in Fig. 7 and proposed in [64], the H-H cell is a single-phase full-bridge controlled rectifier with a single-phase H-bridge inverter. The H-H cell proposes eight switches compared to the ten switches in the conventional regenerative power cell, achieving a reduction of two switches per power cell. The only alteration in the power cell is the grid side inverter and connection that utilize a single-phase source.

Due to the changes in the grid connection, the H-H cell requires a connection with a single-phase transformer and grid filter. This may pose some limitations as a replacement power cell as the conventional power cell utilizes a three-phase grid connection. However, the output inverter does not change from the conventional regenerative power cell, so the modulation and control of the output inverter do not need to be altered [64].

2) EASE AND SIMPLICITY OF AFE CONTROL IMPLEMENTATION

The switching states of the grid side inverter and its output voltage can be seen in Table 4.

The filter inductor voltage, v_L , can be defined by (3) [64].

$$v_L = L_{filter} \frac{di_s}{dt} = v_s - v_{AFE} = v_s - kV_{DC}, \quad (3)$$

where i_s is the cell input current, L_{filter} is the filter inductance, and k is a switching state constant.

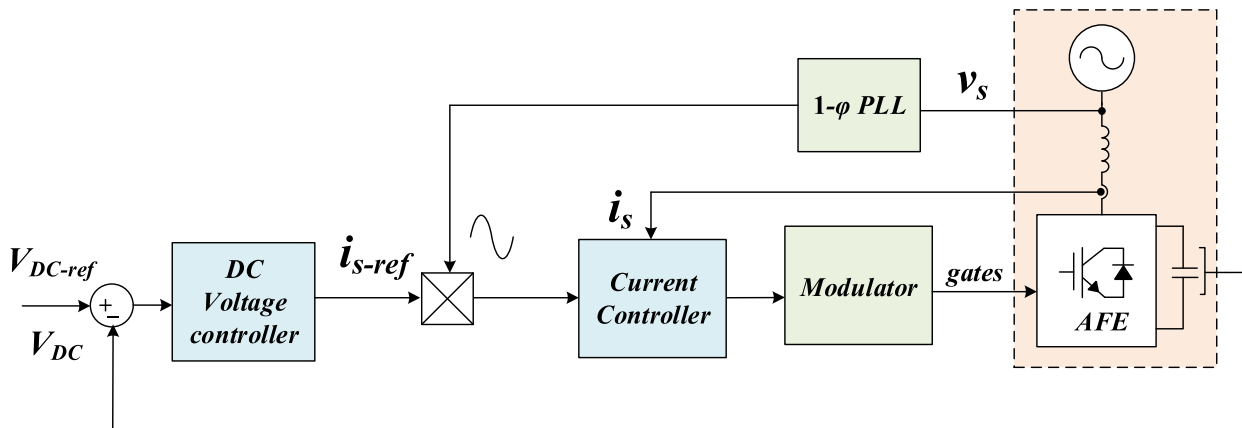


FIGURE 8. FIGURE 1. Control scheme block diagram for H-H cell [64], [68], [70].

TABLE 4. AFE switching states and output voltage.

Switching State	S_1	S_2	V_{AFE}
I	1	0	$+V_{DC}$
II	1	1	0
III	0	0	0
IV	0	1	$-V_{DC}$

Assuming $V_{DC} > V_s$, the behavior of the AFE can be characterized based on Table 5 and (3).

TABLE 5. AFE characteristics based on switching state.

Switching State	v_L	i_s	k
I	Negative	Decreasing	1
II & III	Dependent on v_s	Dependent on v_s	0
IV	Positive	Increasing	-1

Utilizing the characteristics of AFE for the H-H cell, the basic control scheme for the single-phase H-Bridge AFE can be seen in Fig. 8. The DC voltage controller will compare the DC-link voltage (V_{DC}) to the desired reference value (V_{DC-ref}) to set the required active power. The required active power will be multiplied by the sinusoidal waveform of the same phase and frequency given by the PLL to ensure unity power factor operation.

The current controller will produce the required modulation to ensure that the input current tracks the reference.

3) DC-LINK VOLTAGE RIPPLES

The instantaneous power for the H-bridge inverter can be described by (4):

$$\begin{aligned}
 p(t) &= V_1 \sin(\omega t) * I_1 \sin(\omega t - \varphi) \\
 &= \frac{V_1 I_1}{2} (\cos \varphi - \cos(2\omega t - \varphi)), \quad (4)
 \end{aligned}$$

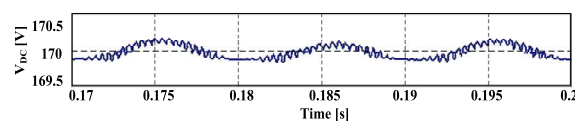


FIGURE 9. H-H cell DC voltage ripples at input and output frequencies of 50 Hz [64].

where V_1 represents the maximum voltage, I_1 represents the maximum current, ω represents the fundamental angular frequency, and φ is the phase shift between the voltage and current. As the H-H cell contains H-bridge inverters on both the input and output, the DC link will contain the pulsating power expressed by (4) from both the input and output sides. As a result, the DC link will experience voltage ripples of double the input frequency ($2\omega_{in}$) and double the output frequency ($2\omega_o$). Fig. 9 shows the DC voltage ripples when input and output frequencies are 50 Hz as shown in [64].

4) CELL INPUT CURRENT HARMONICS

The H-H cell will contain lower order harmonics in the input current in addition to the switching frequency ripples caused by the PWM scheme [64]. As the second-order output ripples are present on the DC-link, this ripple frequency will show in the input currents. As a result, the input current will contain lower-order harmonics described by $(\omega_{in} \pm 2\omega_o)$ and third-order harmonic ripples. Fig. 10 shows the cell input current and its harmonic spectrum when the H-H cell has an input frequency of 50 Hz and output frequency of 10 Hz. The two types of input current harmonics can be observed.

5) COMPLIANCE WITH GRID CONNECTION STANDARDS

The H-H cell can satisfy the grid connection standard by eliminating low order harmonics ($\omega_{in} \pm 2\omega_o$). By configuring three PWM rectifiers as seen in Fig. 11, the low order harmonics in the input current are eliminated as a phase shift of 120° is applied to the cell output pulsating power and resulting ripples in the input currents of the power cells. The carriers of each parallel-connected cell can be shifted by

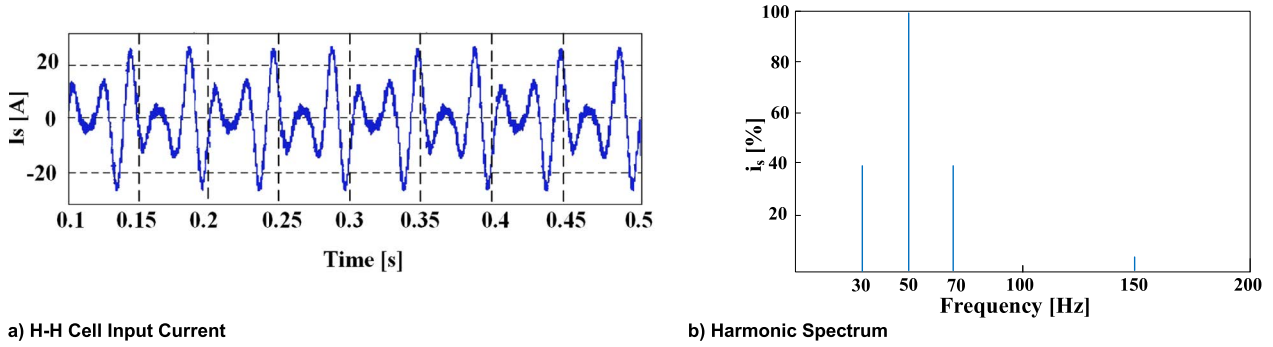


FIGURE 10. H-H Cell Input Current and Harmonic Spectrum at 10 Hz output frequency [64].

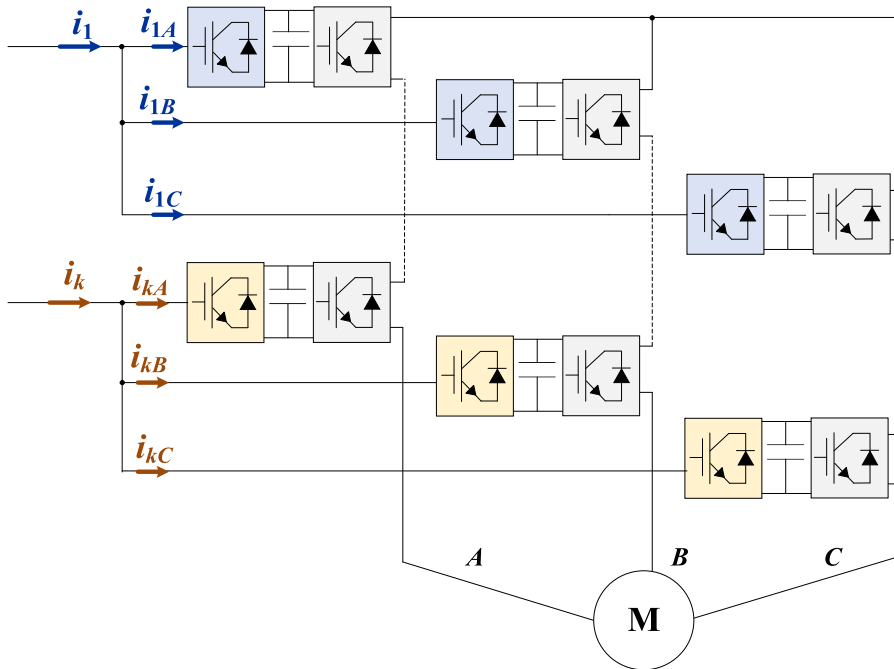


FIGURE 11. Illustration of the required connection for low order harmonic elimination [10], [15].

120° to eliminate the high order switching harmonics [64]. Fig. 12 shows the cell input current and primary current when the output frequency is 20 Hz and the cells are connected as shown in Fig. 11. This low order harmonic elimination method does limit the flexibility of the H-H cell system as the harmonic elimination can only be achieved if the number of cells per phase is a multiple of three [64].

6) SWITCHES RATINGS

The required switch rating can be determined by comparing the conventional power cell to the H-H cell. As the IGBT switches' voltage ratings are based on the DC-link voltage (V_{DC}), it can be seen that the required voltage rating for the switches is equal to V_{DC} in both the conventional and the H-H cell. For the conventional AFE, the maximum RMS output line-to-line voltage utilizing third-order harmonic

injection is described by (5) [14]:

$$V_{l-1,3\phi} = 0.707V_{dc} \tag{5}$$

Comparatively, the maximum RMS output phase voltage from the H-bridge AFE is described by (4) [5]:

$$V_{ph,1\phi} = 0.707V_{dc} \tag{6}$$

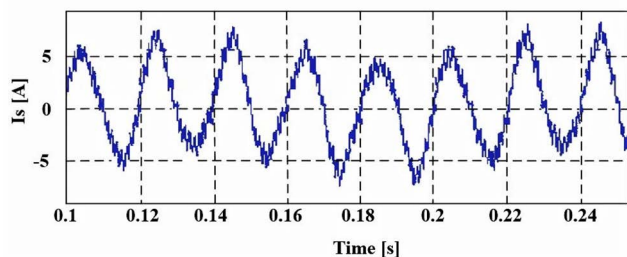
The average power for the conventional and H-H power cells are represented by (5) and (6), respectively:

$$P_{in,3\phi} = \sqrt{3} * V_{l-1,3\phi} * I_{ph,3\phi} \tag{7}$$

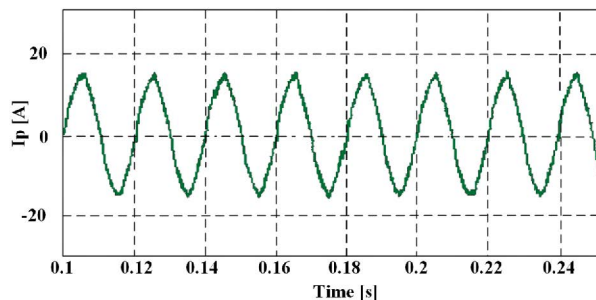
$$P_{in,1\phi} = V_{ph,1\phi} * I_{ph,1\phi} \tag{8}$$

By substituting (5), (6), (7), and (8), the following relationship between the two power cells can be represented by (9):

$$I_{1-\phi} = 1.73I_{ph-3\phi} \tag{9}$$



a) H-H cell input current



b) Primary Current

FIGURE 12. Secondary and primary input currents when output frequency is 20 Hz and cells are connected as shown in Fig. 7 [10].

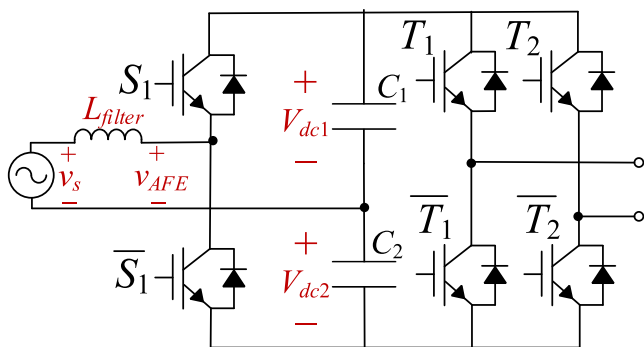


FIGURE 13. Semi-reduced power cell configuration [65], [66].

The relationship between the two power cells indicates that the current ratings of the H-H cell AFE switches should be increased by 73% from the conventional AFE switches to output the same average power.

B. SEMI-REDUCED POWER CELL

1) POWER CELL STRUCTURE

From the H-H cell, a further reduced power cell is proposed in [65] and [66]. The power cell in Fig. 13 proposes a reduction of two switches compared to the H-H cell by utilizing a single-phase half-bridge inverter as AFE rather than an H-Bridge. As the Semi-Reduced power cell maintains the same single-phase AFE and single-phase output configuration as the H-H cell, the power cell requirements and the limitations introduced by the H-H cell apply to the Semi-Reduced Power Cell. The Semi-Reduced cell will require a connection with a single-phase transformer and grid filter. The use of single-phase AFE also introduces limitations with retrofitting as a conventional power cell utilizes a three-phase grid connection.

2) EASE AND SIMPLICITY OF AFE CONTROL IMPLEMENTATION

The Semi-Reduced power cell has two possible switching states, as seen in Table 6:

TABLE 6. AFE switching states and output voltage.

State	S_1	V_{AFE}
I	1	$+V_{dc1}$
II	0	$-V_{dc2}$

The inductor voltage, during state I, can be expressed as seen in (10) [65], [66]:

$$v_L = L_{filter} \frac{di_s}{dt} = v_s - v_{AFE} = v_s - V_{dc1}, \quad (10)$$

where i_s is the cell input current, and L_{filter} is the filter inductance.

During the switching state I, the capacitor charging current and the instantaneous voltages can be expressed by (11) and (12):

$$i_{c1} = i_s - i_l, \quad i_{c2} = -i_l \quad (11)$$

$$v_{dc1} = \frac{1}{C_1} \int i_{c1} dt, \quad v_{dc2} = \frac{1}{C_2} \int i_{c2} dt, \quad (12)$$

where i_l is the input current to the load side H-Bridge.

In the complimentary switching state II, the inductor voltage can be expressed as seen in (13):

$$v_L = L_{filter} \frac{di_s}{dt} = v_s - v_{AFE} = v_s + V_{dc2} \quad (13)$$

The capacitor charging currents can be expressed as (14):

$$\begin{aligned} i_{c1} &= -i_l \\ i_{c2} &= -i_s - i_l \end{aligned} \quad (14)$$

Based on the findings from (11), (12), (13), and (14), the capacitor charging and discharging for the Semi-Reduced Power Cell is seen in Table 7.

Due to the additional complexities regarding capacitor charging and discharging, the control scheme for the H-H cell cannot be used with the Semi-Reduced Power Cell. With the Semi-Reduced Cell, an additional capacitor voltage balancing controller is required for proper control and operation, as seen in Fig. 14.

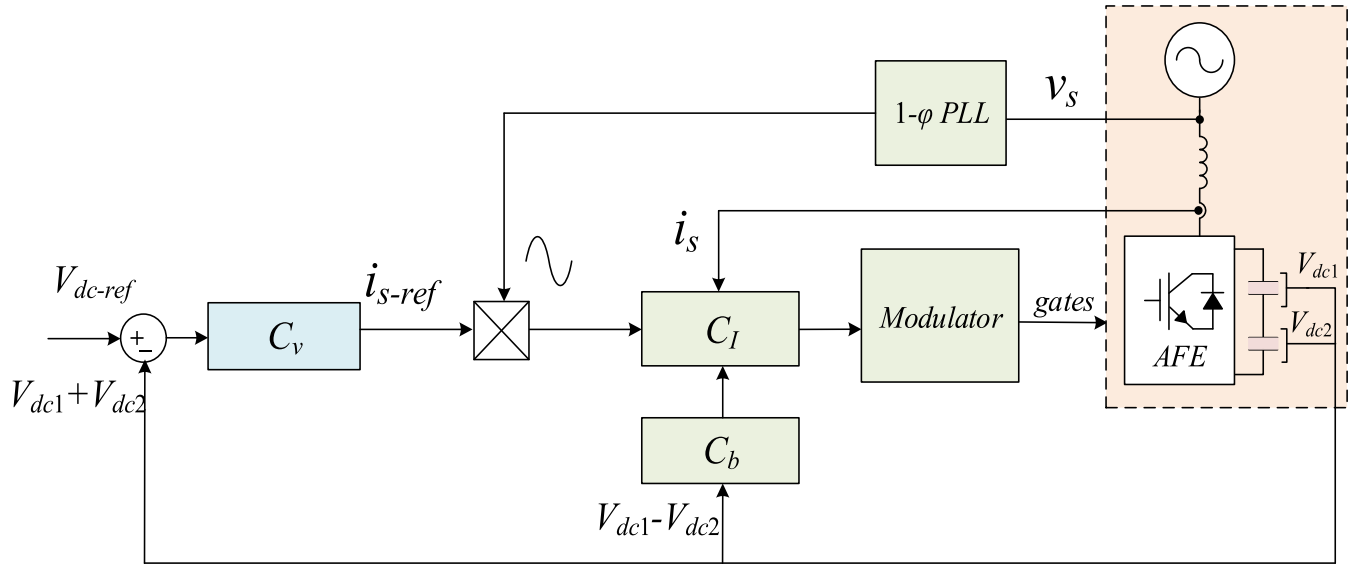


FIGURE 14. Control scheme for semi-reduced power cell [65], [66], [68], [70].

TABLE 7. Capacitor charge and discharge conditions.

Switching State	C ₁	C ₂
I	Charging: (i _s - i _l) > 0 Discharging: (i _s - i _l) < 0	Dependent on i _l
II	Dependent on i _l	Discharging: (i _s + i _l) < 0 Charging: (i _s + i _l) > 0

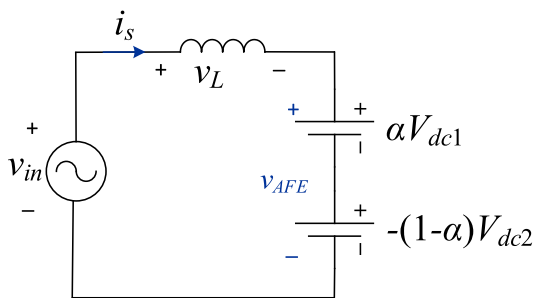


FIGURE 15. Half-bridge average circuit model [12].

3) DC-LINK VOLTAGE RIPPLES

The Semi-Reduced cell suffers from second-order ripples from the output H-Bridge inverter, similar to the conventional and H-H cell. However, the DC-link capacitors also experience fundamental and second-order ripples from the grid side due to the capacitor charging and discharging condition defined by Table 7 [66].

The Half-Bridge AFE can be represented using an average circuit model seen in Fig. 15, where α is the duty cycle ratio

for the upper switch and $(1 - \alpha)$ is the duty cycle ratio for the complimentary switch.

Based on the average circuit model, each capacitor's instantaneous active power can be expressed by (15) and (16) under unity power factor operation [66].

$$\begin{aligned}
 p_{c1}(t) &= \alpha V_{dc1} * i_s = \alpha V_{dc1} * I_s \sin(\omega_{int}) \\
 &= V_{dc1} \left(\frac{V_{AFE} I_s}{2V_{dc}} (\cos(\delta) - \cos(2\omega_{int} - \delta)) \right. \\
 &\quad \left. + \frac{I_s}{2} \sin(\omega_{int}) \right) \tag{15}
 \end{aligned}$$

$$\begin{aligned}
 p_{c2}(t) &= -(1 - \alpha)V_{dc2} * i_s \\
 &= V_{dc2} \left(\frac{V_{AFE} I_s}{2V_{dc}} (\cos(\delta) - \cos(2\omega_{int} - \delta)) \right. \\
 &\quad \left. - \frac{I_s}{2} \sin(\omega_{int}) \right), \tag{16}
 \end{aligned}$$

where V_{dc1} is the average voltage of c_1 , V_{dc2} is the average voltage of c_2 , V_{AFE} is the magnitude of the AFE output voltage, I_s is the magnitude of the grid current, V_{dc} is the voltage of the DC link, ω_{in} is the angular frequency of the grid and δ is the phase shift from the AFE output and the grid voltage.

As capacitors experience voltage harmonics, the same as power harmonics, (15) and (16) demonstrate the existence of input fundamental and second-order voltage ripples as shown in Fig. 16(a). However, due to the configuration of the capacitors in the Semi-Reduced power cell, the total DC-Link voltage will be subjected to second-order harmonics only, Fig. 16(b), as the fundamental ripples are 180° out of phase [66].

4) CELL INPUT CURRENT HARMONICS

Similar to the H-H cell, the Semi-Reduced power cell will experience second-order harmonic ripples due to the voltage

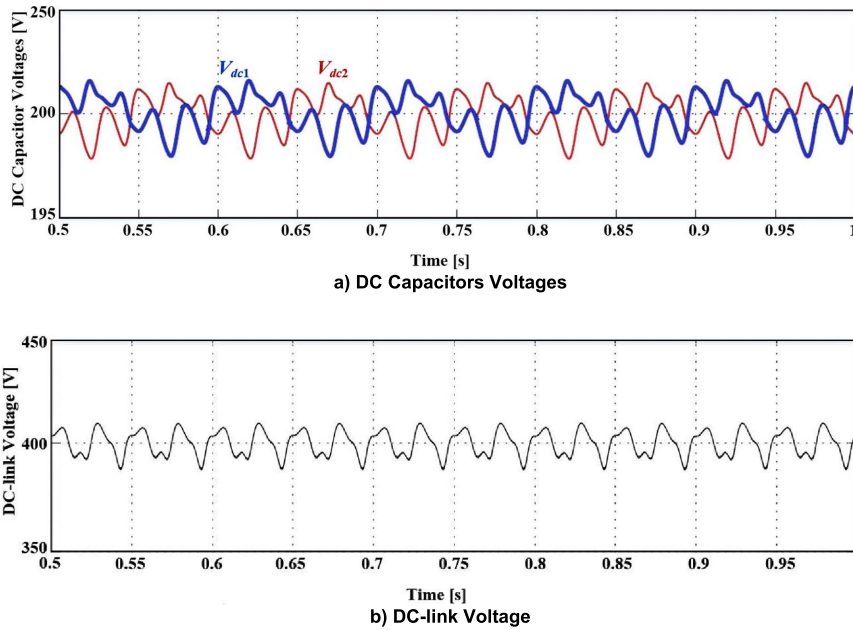


FIGURE 16. DC-capacitors and DC-link voltages for semi-reduced cell shown in [12].

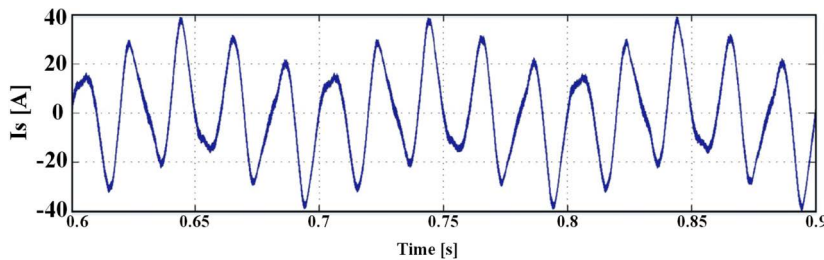


FIGURE 17. Semi-reduced cell input current with 50 Hz input frequency and 20 Hz output frequency as shown in [12].

ripples in the capacitors and lower-order harmonics as shown in Fig. 17. Additionally, higher-order harmonic ripples from SPWM switching will be present [65], [66], [68].

5) COMPLIANCE WITH GRID CONNECTION STANDARDS

The Semi-Reduced cell can satisfy the grid connection standard by utilizing the same interconnection as the H-H cell, as seen in Fig. 11. In [66], an additional interconnection, shown in Fig. 18, is used to satisfy the grid connection standards, as seen in Fig. 10. The interconnection is similar to the interconnection used in the H-H cell. However, the transformer is a three-phase transformer with separate single-phase secondary winding. The low order harmonics in the primary input current are eliminated by applying a 120° phase shift to the capacitor voltage ripples in each row of power cells. Fig. 19 shows the input primary current using Fig. 18 interconnection.

Similar to the H-H cell, the low order cancellation method is only effective when the number of cells per phase is a multiple of three [65], [66].

6) SWITCHES RATING

The analysis completed with the H-H cell can be used on the Semi-Reduced cell to determine the required switch rating. As the H-Bridge output is double the half-bridge output, the following conclusion can be made for the Semi-Reduced power cell’s maximum RMS output phase voltage:

$$V_{ph,half-bridge} = 0.35V_{dc} \tag{17}$$

The input power can be represented, as seen in (18):

$$P_{half-bridge} = V_{ph,half-bridge} * I_{ph,half-bridge} \tag{18}$$

Taking (17) and (18), the relationship between a 2L-VSI and the Semi-Reduced power cell can be represented by (19):

$$I_{ph,half-bridge} = 3.46I_{ph,3\phi} \tag{19}$$

The relationship derived from (19) illustrates that the current rating of the switches for the Semi-Reduced cell needs to increase by 246% compared with a 2L-VSI.

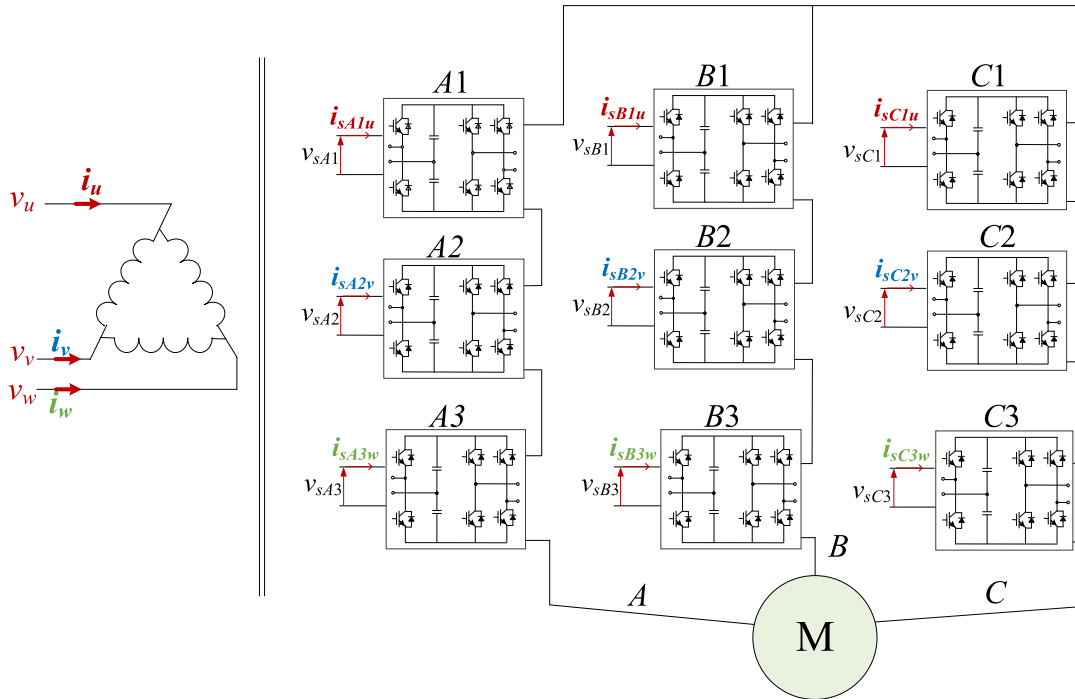


FIGURE 18. Interconnection of 7-level CHB semi-reduced cells [66], [70].

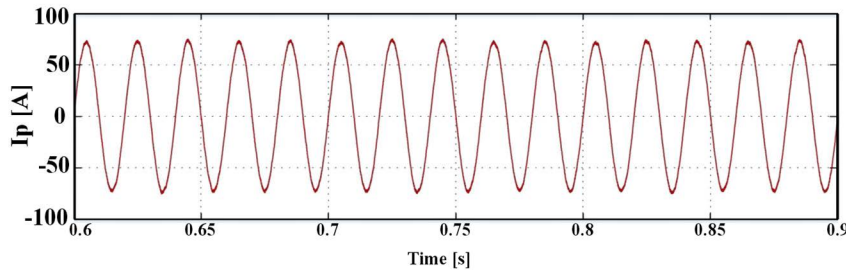


FIGURE 19. Primary input current using Fig. 14 interconnection as shown in [12].

C. REDUCED POWER CELL

1) POWER CELL STRUCTURE

In [67], a power cell with the least switch-count is proposed. The H-Bridge output inverter is converted to a half-bridge inverter compared to a Semi-Reduced power cell, and the total switch count reduces to four. The reduced power cell can be seen in Fig. 20. As the reduced power cell is a further reduction from the H-H cell and the semi-reduced power cell, the limitation imposed by the structure of the previously analyzed power cells applies to the reduced power cell.

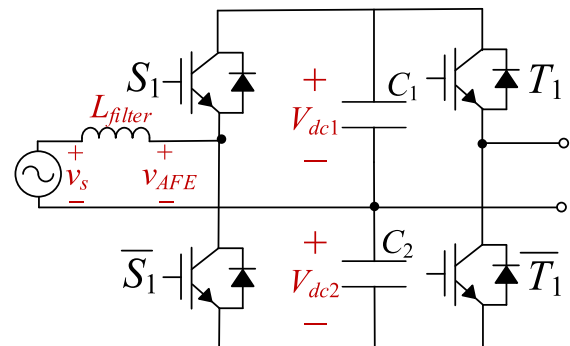


FIGURE 20. Reduced cell power cell configuration [67].

2) EASE AND SIMPLICITY OF AFE CONTROL IMPLEMENTATION

The reduced power cell proposes the same AFE structure as the semi-reduced power cell. As a result, the findings are shown in Table 6, and 7 remain the case for the reduced power cell. The control scheme, seen in Fig. 14, is required for this power cell's proper control and operation.

3) DC-LINK VOLTAGE RIPPLES

The analysis conducted for the Semi-Reduced cell can be used to determine the DC-Link voltage ripples for the Reduced cell. Using the average model, as seen in Fig. 15,

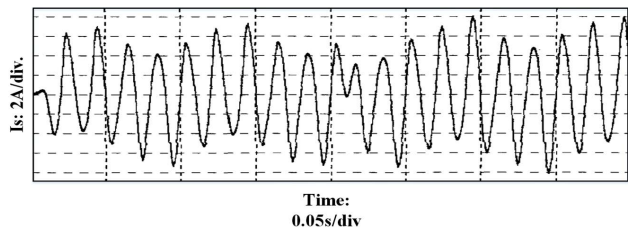


FIGURE 21. Reduced cell input current for 50 Hz grid frequency and 20 Hz output frequency, as shown in [67].

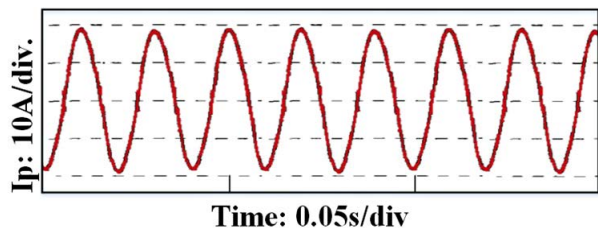


FIGURE 22. Reduced cell primary input current as shown in [67].

the instantaneous powers for both capacitors can be described by (20) and (21), as shown at the bottom of the page, [70], where α_{in} and α_o are the inverter input and output duty ratios, respectively. V_{dc1} and V_{dc2} are the average voltage of c_1 and c_2 , V_{AFE} is the magnitude of the AFE output voltage, I_s is the magnitude of the grid current, V_{dc} is the voltage of the DC link, ω_{in} is the angular frequency of the grid, ω_o is the angular frequency of the output, δ_{in} is the phase shift between the AFE voltage and current, and ϕ_o is the phase shift between the output voltage and current.

From (20) and (21), both capacitors in the Reduced cell will consist of fundamental and second-order harmonic ripples from both input and output. However, due to the phase shift of the fundamental harmonic ripple between the two capacitors, the total DC-link will only contain second-order harmonics from the input and output of the cell.

4) CELL INPUT CURRENT HARMONICS

As the Reduced cell share the same input configuration as the Semi-Reduced cell, the harmonics in the input current remain similar. The second-order harmonic ripples are reflected from

the capacitors' voltages to the input current, in addition to the higher-order harmonic ripples from the SPWM switching [67]. Fig. 2 shows the cell input current for 50 Hz input frequency and 20 Hz output frequency as shown in [67].

5) COMPLIANCE WITH GRID CONNECTION STANDARDS

The same interconnection shown in Fig. 11 and Fig. 18 can be utilized to cancel the lower-order harmonics in the primary currents. As with the previous cells analyzed, the number of cells per phase must be a multiple of three for the interconnections to be effective [67]. Fig. 22 shows the input primary current when the interconnections are used as shown in [67].

6) SWITCHES RATINGS

The Reduced cell replaces the H-bridge output inverter with a half-bridge inverter to reduce the switch count. For the Reduced cell to generate the same voltage output, the DC-link must be increased by 100%. The voltage ratings of all switches must be doubled compared to the conventional 10-switch regenerative power cell.

With the DC-link voltage doubled, the relationship between a 2L-VSI and the Reduced cell AFE can be represented by (22):

$$I_{ph,half-bridge} = \frac{3.46}{2} I_{ph,3\phi} \quad (22)$$

Therefore, the AFE switches current rating for the Reduced cell will be 73% higher compared to the 2L-VSI switches.

D. COMMENTS ON THE EXISTING SINGLE-PHASE AFE REDUCED SWITCH-COUNT POWER CELLS

The review of the existing single-phase AFE reduced switch-count power cells demonstrates the feasibility of single-phase reduced switch-count power cells. However, reducing the number of switches proposes many challenges [64]–[68]:

- A single-phase AFE interface allows the use of a simpler transformer. However, the control for single-phase AFE is more complex than three-phase.
- The DC-Link voltage will contain second-order harmonics from both input and output. For Semi-Reduced and Reduced cells, fundamental voltage ripples are present in the individual capacitors.

$$p_{c1}(t) = \alpha_{in} V_{dc1} * i_s + \alpha_o V_{dc1} * i_o$$

$$= V_{dc1} \left[\begin{aligned} &\left(\frac{V_{AFE} I_s}{2V_{dc}} (\cos(\delta_{in}) - \cos(2\omega_{in}t - \delta_{in})) + \frac{I_s}{2} \sin(\omega_{in}t) \right) \\ &+ \left(\frac{V_o I_o}{2V_{dc}} (\cos(\phi_o) - \cos(2\omega_o t - \phi_o)) + \frac{I_o}{2} \sin(\omega_o t) \right) \end{aligned} \right] \quad (20)$$

$$p_{c2}(t) = -(1 - \alpha_{in}) V_{dc2} * i_s - (1 - \alpha_o) V_{dc2} * i_o$$

$$= V_{dc2} \left[\begin{aligned} &\left(\frac{V_{AFE} I_s}{2V_{dc}} (\cos(\delta_{in}) - \cos(2\omega_{in}t - \delta_{in})) - \frac{I_s}{2} \sin(\omega_{in}t) \right) \\ &+ \left(\frac{V_o I_o}{2V_{dc}} (\cos(\phi_o) - \cos(2\omega_o t - \phi_o)) - \frac{I_o}{2} \sin(\omega_o t) \right) \end{aligned} \right], \quad (21)$$

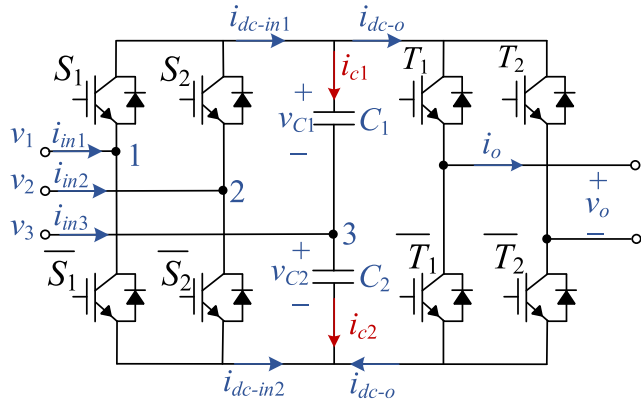


FIGURE 23. Three-phase reduced switch-count power cell [69].

- The harmonics present can only be eliminated if the number of cells per phase is a multiple of three.
- The capacitors in Semi-Reduced and Reduced cells can experience voltage imbalance due to manufacturing and operation differences.
- The output voltage level for the Reduced cell is $(n + 1)$ compared to $(2n + 1)$ levels, where n represents the number of cells per phase.
- The switches' voltage ratings are doubled for the Reduced cell configurations.

The existing single-phase AFE reduced switch-count power cells successfully reduce the number of switches per power cell. However, as the use of single-phase AFE introduces complex control, low order harmonics, and DC-link ripples, the practical implementation of the proposed power cells does introduce challenges.

IV. REVIEW OF THREE-PHASE REDUCED SWITCH COUNT POWER CELLS

Three-phase AFEs provide a more straightforward control than single-phase AFEs as a rotating $d-q$ reference frame can help in the control scheme. Moreover, low order harmonics from the input primary currents can be canceled without any limitation imposed by the cell numbers, making three-phase reduced switch count cells a more suitable option for practical implementation. A three-phase reduced switch count cell is proposed in [69], as seen in Fig. 23.

A. POWER CELL STRUCTURE

The Reduced Switch-Count cell introduced in [69] reduces the number of switches by two per cell by replacing the 2L-VSI with a Four-Switch Three-Phase Inverter (FSTPI). As the proposed cell maintains the three-phase input and a single-phase output structure as the conventional regenerative power cell, the three-phase grid connection is maintained. The output inverter does not change from the conventional regenerative power cell, so the modulation and control of the output inverter do not need to be altered.

B. EASE AND SIMPLICITY OF AFE CONTROL IMPLEMENTATION

The FSTPI used in the Reduced Switch-Count cell confines one phase to the DC-link midpoint. As a result, only four switching states exist, as seen in Table 8 [71]. The possible switching states give the output voltage vector defined by:

$$\bar{v} = \frac{2}{3} \left(S_1 * V_{dc} + S_2 * V_{dc} * e^{i\frac{2\pi}{3}} + \frac{V_{dc}}{2} * e^{-i\frac{2\pi}{3}} \right) \quad (23)$$

TABLE 8. AFE switching states and output.

Vector	Switching State		Voltage Vector	
	S_1	S_2	Magnitude	Angle
V_1	0	0	$V_{dc}/\sqrt{3}$	-30°
V_2	1	1	$V_{dc}/3$	60°
V_3	0	1	$V_{dc}/\sqrt{3}$	150°
V_4	0	0	$V_{dc}/3$	240°

As the FSTPI has one phase connected to the midpoint of the capacitor, the SPWM modulation of the other phases must be modified from (24) to (25) for proper control and operation [73].

$$v_{1-ref} = V \sin(\omega t), v_{2-ref} = V \sin(\omega t - \frac{2\pi}{3})$$

$$v_{3-ref} = V \sin(\omega t + \frac{2\pi}{3}) \quad (24)$$

$$v_{1o-ref} = v_{13} = v_{1-ref} - v_{3-ref} = \sqrt{3} V \sin(\omega t - \frac{\pi}{6})$$

$$v_{2o-ref} = v_{23} = v_{2-ref} - v_{3-ref} = \sqrt{3} V \sin(\omega t - \frac{\pi}{2}) \quad (25)$$

With the previous modification to the modulation signal, the carrier signal should be multiplied by $\sqrt{3}$ due to the amplitude of the new modulating signals. The control scheme for the three-phase reduced switch-count power cell can be seen in Fig. 24.

C. DC-LINK VOLTAGE RIPPLES

The instantaneous capacitor voltage of the Reduced Switch-Count cell can be expressed by (26):

$$i_{dc-in1} = \frac{I_{in}}{2} \sin(\omega_{in}t - \theta - \frac{\pi}{3}) + \frac{\sqrt{3}}{4} m_{in} * I_{in} * \cos \theta$$

$$i_{dc-in2} = \frac{I_{in}}{2} \sin(\omega_{in}t - \theta - \frac{\pi}{3}) - \frac{\sqrt{3}}{4} m_{in} * I_{in} * \cos \theta \quad (26)$$

Considering the instantaneous capacitor voltage defined by (2), the currents for the capacitors can be defined by (27) and (28) [71]–[73]:

$$i_{c1} = i_{dc-in1} - i_{dc-o}$$

$$= \frac{\sqrt{3}}{4} m * I_{in} * \cos \theta + \frac{I_{in}}{2} \sin(\omega_{in}t - \theta - \frac{\pi}{3}) - m_o * I_o [\cos \phi_o + \cos(2\omega_o t - \phi_o)] \quad (27)$$

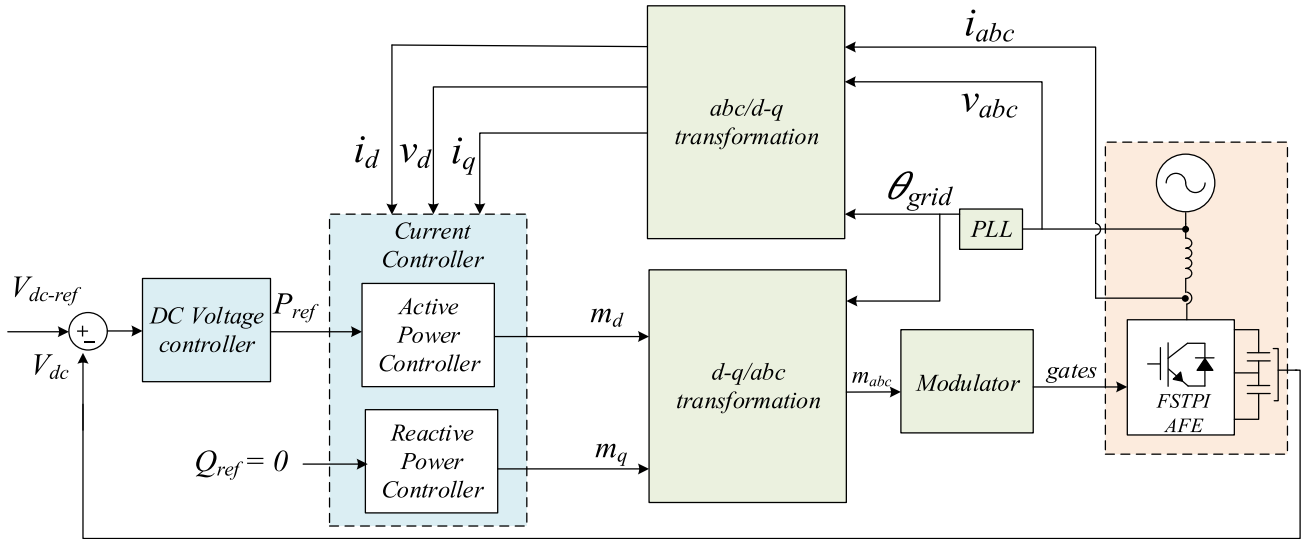


FIGURE 24. Control scheme for three-phase reduced switch-count cell [69], [71], [72], [73].

$$\begin{aligned}
 i_{c2} &= -i_{dc-in2} - i_{o-dc} \\
 &= \frac{\sqrt{3}}{4} m * I_{in} * \cos \theta - \frac{I_{in}}{2} \sin \left(\omega_{in} t - \theta - \frac{\pi}{3} \right) \\
 &\quad - m_o * I_o [\cos \phi_o + \cos(2\omega_o t - \phi_o)], \quad (28)
 \end{aligned}$$

where m_{in} is the modulation index of the AFE inverter, m_o is the modulation index of the output inverter, I_{in} is the input current fundamental magnitude, I_o is the output current fundamental magnitude, θ is the phase shift between the FSTPI output fundamental phase voltage and current and ϕ_o is the phase shift between the H-bridge output fundamental phase voltage and current.

Each capacitor will experience voltage ripples of input fundamental frequency (ω_{in}) due to the connection of the DC-link midpoint. However, the ripples across the two capacitors are 180° apart, and as a result, these ripples cancel each other when observing the whole DC-link voltage [71].

The H-bridge output inverter will introduce voltage ripples of output second-order harmonic frequency ($2\omega_o$) due to the pulsating power. As each capacitor's second-order voltage ripples are in phase, the voltage ripple will appear on the total DC-link voltage. In addition, the DC-link voltage will experience switching harmonics from both input and output inverters.

Fig. 25 shows the individual DC-capacitors and total DC-link voltages as shown in [71].

D. CELL INPUT CURRENT HARMONICS

Due to the capacitor ripples present in the three-phase reduced switch count power cell, the FSTPI input line currents contain lower-order harmonics. The DC-link ripples of $2\omega_o$ frequency inject ripples of $(\omega_{in} \pm 2\omega_o)$ frequencies into the input current. However, due to the three-phase interface of the FSTPI, the low-order harmonics seen in the input of the power cells will not be observed in the primary side of the

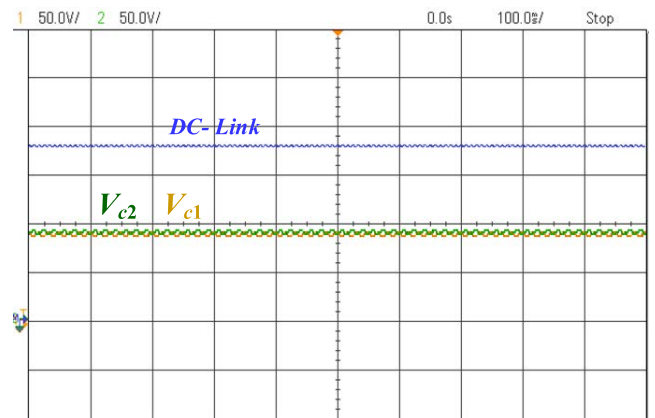


FIGURE 25. DC-capacitors and total DC-link voltages as shown in [71].

transformer for any number of cells per phase. The primary current of the transformer with unity turns ratio can be represented by (2) when the power cells are configured, as seen in Fig. 26.

$$I_{p-k} = \sum_{j=1}^n I_{sk-Aj} + I_{sk-Bj} + I_{sk-Cj}, \quad (29)$$

where k is the grid phase index ($u, v,$ and w), j is the row number index, p stands for primary, and s stands for secondary.

If the FSTPI is configured as seen in Fig. 26, the low-order harmonics ripples in the secondary input currents for each drive phase cell will be phase-shifted by 120° . According to (29), the low-order harmonics on the primary side of the transformer will equal zero for any number of cells [71].

E. COMPLIANCE WITH GRID CONNECTION STANDARDS

In addition to the low order harmonics observed at the input of the power cell, the reduced switch count cell suffers from

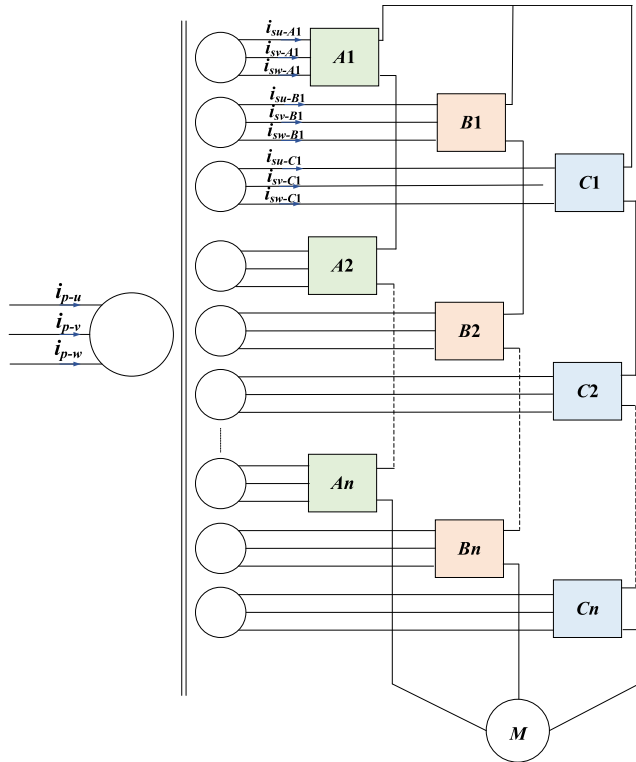


FIGURE 26. Low order harmonic cancellation configuration [70].

current unbalance due to the fundamental voltage ripples in each capacitor. The current unbalances observed on the secondary side of the transformer will not cancel with the configuration seen in Fig. 26. A phase alternation method, shown in Fig. 23, can ensure that the unbalance observed on the secondary side of the transformer is canceled on the primary side [69].

By alternating the DC-link midpoint connection with each phase group, the fundamental capacitors' ripples and the resulting unbalance are shifted by 120°, canceling out on the primary side. The alternation method additionally cancels triplen and carrier harmonic components, ensuring that the input currents observed on the primary side are balanced and without low order harmonics present. Fig. 28 shows the primary input currents and their harmonic spectrum for the connections in Fig. 26 and 27 as presented in [71].

F. SWITCHES RATINGS

As the three-phase reduced switch-count power cell utilizes an H-bridge inverter in the output, the voltage rating remains the same as the 2L-VSI. The maximum RMS line-to-line voltage of the FSTPI utilizing third-order harmonic injection can be described by (30) [72].

$$V_{l-l, FSTPI} = 0.4V_{dc} \quad (30)$$

Evaluating the current relationship between the 2L-VSI and FSTPI based on power, (31) can be derived [72].

$$I_{FSTPI} = 1.77I_{ph,3\phi} \quad (31)$$

The current relationship, seen by (31), demonstrates that the current ratings for the FSTPI should be increased by 77% compared to the 2L-VSI. However, due to the existing harmonics on the input cell currents, the current rating of the switches should be doubled.

1) COMMENTS ON THE EXISTING THREE-PHASE AFE REDUCED SWITCH-COUNT POWER CELL

The FSTPI-based regenerative power cell offers the advantages of the three-phase front end of simpler control and low order harmonic elimination. However, the DC-link voltage input fundamental ripples, the low DC-link utilization factor, and high switches' current ratings are still remaining challenges that need to be addressed [72].

V. DESIGN CONSIDERATION

The review of the existing reduced switch-count regenerative power cells draws the attention to the importance of considering the design challenges associated with the switch-count reduction. To keep the same power, the voltage and current stresses increase. In addition, the reduction of switches number leads to more low harmonic ripple stresses on the DC-link capacitors which affect the capacitors' lifetime [71], [74].

One way to estimate the reliability probability density function is using the bottom-up approach. For an item consisting of n parts, where the failure of one of the parts leads to the failure of the whole item and there is no interaction between the parts' failures, the resultant item reliability density function $R(t)$ is modeled as [75]:

$$R(t) = R_1(t) * R_2(t) * \dots * R_n(t), \quad (32)$$

where $R_x(t)$ is the reliability probability density function of part x and is less than 1.

Based on (32) it can be concluded that by reducing the numbers of switches, the accompanying gate drivers and control circuits, the AFE converter failure probability caused by the failure of these components can be decreased.

Nevertheless, the increased stresses on other components such as capacitors while reducing the number of switches may compromise the long-term converter's reliability [74], [75].

VI. COMPARISON OF REDUCED SWITCH-COUNT POWER CELLS WITH CONVENTIONAL REGENERATIVE CELL

Table 9 summarizes the comparison between conventional regenerative power cells and the reduced switch-count power cells.

Based on the review of the reduced switch-count power cells, each reduced switch-count topology demonstrates the criteria of a successful design defined in this paper. Utilizing a single-phase AFE design can provide a regenerative power cell with the least switch count, while utilizing a three-phase AFE design is able to provide a solution that is easier to implement than the single-phase AFE design.

The H-H cell and the Semi-Reduced cell provide a switch count reduction of two and four, respectively. The two designs

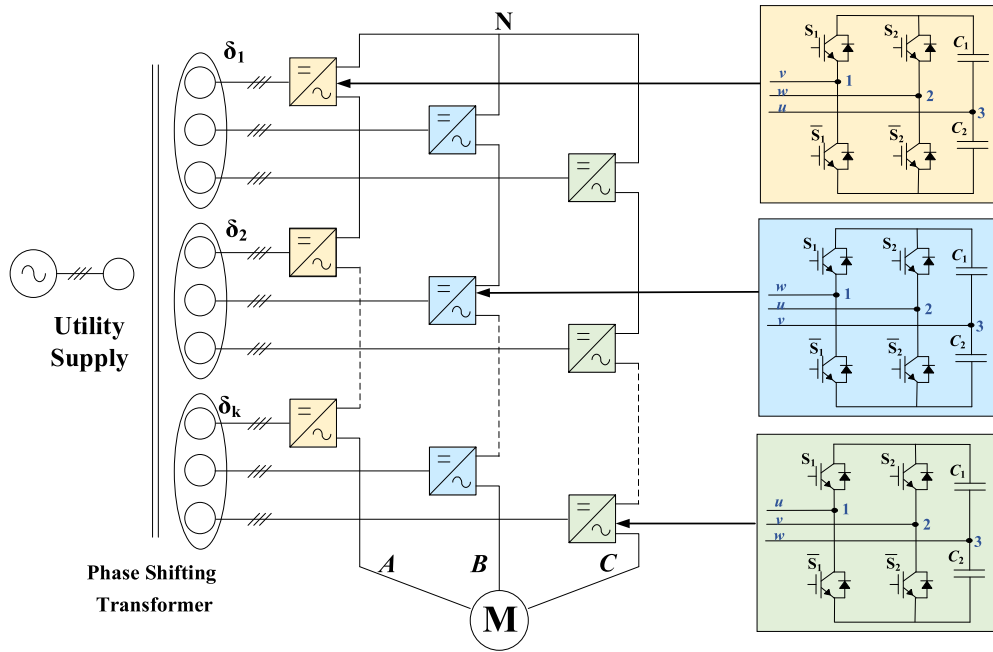


FIGURE 27. Proposed phase alternation method [70].

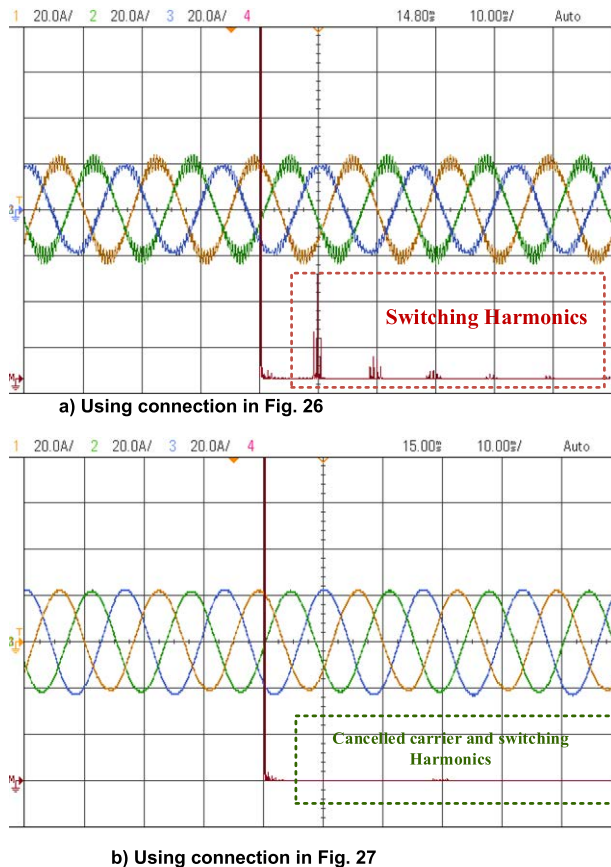


FIGURE 28. Input primary current as resulted from [71] experimental results.

can achieve the reduction with the use of a single-phase AFE design. A single-phase AFE proposes a more complex

controller design as a stationary *abc* frame must be used and provides a solution that can only meet the grid harmonics standards in a multiple of three cells per phase. With each reduction of switches, the current rating of the switches needs to be increased. The reduced cell design provides a switch count reduction of six compared to the conventional regenerative power cell. The reduced cell achieves the switch-count reduction by using a half-bridge AFE inverter, similar to the Semi-Reduced cell but also utilizing a half-bridge inverter on the output. This results in a regenerative power cell with the least switch count. However, the reduced cell still requires a complex controller design, and low order harmonic elimination can only be accomplished in a multiple of three cells per phase. In addition, the reduced cell can only provide $(n + 1)$ output levels due to the output inverter reduction while requiring a higher switch current rating and double the voltage rating.

The three-phase Reduced Switch-Count Regenerative cell provides a switch count reduction of two. The design is able to achieve the reduction by utilizing an FSTPI AFE inverter. As the design maintains a three-phase AFE, a simple controller can be used and can meet the grid harmonic for any number of cells per phase. Similar to the single-phase reduced switch-count cells, the reduction of two switches in the Reduced Switch-Count Regenerative cell requires that the current ratings for the AFE switches be increased.

The switch-count reduction leads to the reduction of the switches' associated costs as can be seen in the table. However, the AFE power losses correlation is not straightforward. As the conduction losses are directly proportional to the square of the cell input current [76], these losses will increase with the increases current rating to keep the same power in the reduced switch-count power cells. On the other

TABLE 9. Comparison of reduced switch count cells referred to conventional regenerative power cell [71].

Cell Configuration	Three-Phase Power Cell		Single-Phase Power Cell		
	Conventional 10-Switch Regenerative Cell	Reduced Switch-Count Regenerative Cell	H-H Cell	Semi-Reduced Cell	Reduced Cell
Number of Switches	10	8	8	6	4
Output Voltage Levels	$2n+1$	$2n+1$	$2n+1$		$n+1$
AFE Interface	Three-phase		Single-phase		
AFE Control Frame	Rotating $d-q$		Stationary abc (more complex)		
Low order harmonic elimination	Effective for any number of cells/phase		Effective only if number of cells/phase is multiple of three		
Low order DC-link ripples	Output 2 nd order		Output and input 2 nd order		
Capacitor ripples	Output 2 nd order	Output 2 nd order	Output and input 2 nd order		
		Input fundamental	-	Input Fundamental	
		-	-	-	Output fundamental
AFE Switches current rating	I_{in}	$2I_{in}$	$1.73I_{in}$	$3.46I_{in}$	$1.73I_{in}$
Switches voltage ratings	V_{dc}		V_{dc}		$2V_{dc}$
Cells Switches' Cost	100%	80%	80%	60%	40%
AFE Switches' Conduction Losses	100%	400%	300%	1197%	300%
AFE Switches' Switching Losses	100%	80%	80%	60%	40%

hand, the switching losses are more coupled with the switching frequency and number of switches, therefore these losses will be reduced with the reduction of the switch-count [76]. Therefore, there is a trade-off between switch reduction and conduction losses.

VII. FUTURE TRENDS

Further switch-count reduced topologies can be investigated. Based on the analysis of the single-phase and three-phase reduced switch-count power cell designs, the three-phase reduced switch-count power cell can be improved to minimize the switch count further. In the single-phase cell designs, the Reduced cell provided an additional switch count reduction of two by utilizing a half-bridge inverter on the output. A three-phase regenerative power cell with six switches can be a good candidate by utilizing the FSTPI for AFE, and a half-bridge inverter for the output. The use of an FSTPI provides a simple controller design and flexible low order harmonic elimination method evident with the Reduced Switch-Count Regenerative Cell. The half-bridge inverter will allow a design of a three-phase regenerative power cell with the least switch count. However, similar to the Reduced cell, the proposed power cell requires a higher current rating, double the voltage rating, and provides less output voltage levels than the power cells with an H-Bridge output inverter.

While the controller design will be simpler compared to the single-phase reduced switch-count power cell, there will be an additional challenge as the half-bridge output inverter will introduce output fundamental voltage ripples in the DC-link. This ripple component will affect the operation and stability of the rotating $d-q$ frame controller and introduce unbalance in the system. However, with the challenge addressed, this power cell should meet the criteria set out in this paper for a successful design and provide a three-phase reduced switch-count power cell with the least switch count.

Another aspect that can be looked at is new control techniques that can reduce the DC-link capacitor ripple stresses to improve the capacitors' lifetime [77].

The advancement in the semiconductor technologies with the wide bandgap devices (GaN and SiC) provides new potentials to withstand the high current and voltage ratings with lower conduction resistance and switching losses [78].

VIII. CONCLUSION

This paper presented a comprehensive review of the existing single-phase and three-phase reduced switch-count power cell designs for the regenerative Cascaded H-Bridge motor drives applications. Each power cell design is evaluated against the conventional 10-switch regenerative power cell to determine the advantages and disadvantages regarding

structure, control, and harmonics present in the system. The key characteristics of the power cells are summarized to identify the requirements and differences between all regenerative power cells presented in this paper. Additionally, a new possible configuration is proposed to reduce the existing three-phase reduced switch-count power cell.

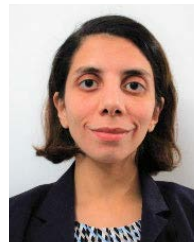
REFERENCES

- [1] H. Akagi, "Multilevel converters: Fundamental circuits and systems," *Proc. IEEE*, vol. 105, no. 11, pp. 2048–2065, Nov. 2017, doi: 10.1109/JPROC.2017.2682105.
- [2] S. Ahmad, S. H. Johari, A. Ahmad, and M. F. M. A. Halim, "Grid connected multilevel inverters for PV application," in *Proc. IEEE Conf. Energy Convers. (CENCON)*, Johor Bahru, Malaysia, Oct. 2015, pp. 181–186, doi: 10.1109/CENCON.2015.7409536.
- [3] M. Trabelsi, H. Vahedi, and H. Abu-Rub, "Review on single-DC-source multilevel inverters: Topologies, challenges, industrial applications, and recommendations," *IEEE Open J. Ind. Electron. Soc.*, vol. 2, pp. 112–127, 2021, doi: 10.1109/OJIES.2021.3054666.
- [4] V. Patel, M. Tinari, C. Buccella, and C. Cecati, "Analysis on multilevel inverter powertrains for E-transportation," in *Proc. IEEE 13th Int. Conf. Compat., Power Electron. Power Eng. (CPE-POWERENG)*, Sonderborg, Denmark, Apr. 2019, pp. 1–6, doi: 10.1109/CPE.2019.8862373.
- [5] J. Rodríguez, J.-S. Lai, and F. Z. Peng, "Multilevel inverters: A survey of topologies, controls, and applications," *IEEE Trans. Ind. Electron.*, vol. 49, no. 4, pp. 724–738, Aug. 2002.
- [6] S. Kouro, M. Malinowski, K. Gopakumar, J. Pou, L. G. Franquelo, B. Wu, J. Rodríguez, M. A. Pérez, and J. I. Leon, "Recent advances and industrial applications of multilevel converters," *IEEE Trans. Ind. Electron.*, vol. 57, no. 8, pp. 2553–2580, Aug. 2010.
- [7] K. K. Gupta and S. Jain, "Comprehensive review of a recently proposed multilevel inverter," *IET Power Electron.*, vol. 7, no. 3, pp. 467–479, Mar. 2014.
- [8] A. Nami, L. Jiaqi, F. Dijkhuizen, and G. D. Demetriades, "Modular multilevel converters for HVDC applications: Review on converter cells and functionalities," *IEEE Trans. Power Electron.*, vol. 30, no. 1, pp. 18–36, Jan. 2015.
- [9] S. Debnath, J. Qin, B. Bahrani, M. Saeedifard, and P. Barbosa, "Operation, control, and applications of the modular multilevel converter: A review," *IEEE Trans. Power Electron.*, vol. 30, no. 1, pp. 37–53, Jan. 2015.
- [10] D. Ronanki and S. S. Williamson, "Modular multilevel converters for transportation electrification: Challenges and opportunities," *IEEE Trans. Transport. Electrific.*, vol. 4, no. 2, pp. 399–407, Jun. 2018.
- [11] M. N. Raju, J. Sreedevi, R. P. Mandi, and K. S. Meera, "Modular multilevel converters technology: A comprehensive study on its topologies, modelling, control and applications," *IET Power Electron.*, vol. 12, no. 2, pp. 149–169, Feb. 2019.
- [12] M. A. Perez, S. Bernet, J. Rodriguez, S. Kouro, and R. Lizana, "Circuit topologies, modeling, control schemes, and applications of modular multilevel converters," *IEEE Trans. Power Electron.*, vol. 30, no. 1, pp. 4–17, Jan. 2015.
- [13] M. Priya, P. Ponnambalam, and K. Muralikumar, "Modular-multilevel converter topologies and applications - a review," *IET Power Electron.*, vol. 12, no. 2, pp. 170–183, 2019.
- [14] B. Wu and M. Narimani, *High-Power Converters and AC Drives*, 2nd ed. Hoboken, NJ, USA: Wiley, 2017, pp. 119–140.
- [15] M. S. Diab, A. M. Massoud, S. Ahmed, and B. W. Williams, "A dual modular multilevel converter with high-frequency magnetic links between sub-modules for MV open-end stator winding machine drives," *IEEE Trans. Power Electron.*, vol. 33, no. 6, pp. 5142–5159, Jun. 2018.
- [16] R. V. Nair, K. Gopakumar, and L. G. Franquelo, "A very high resolution stacked multilevel inverter topology for adjustable speed drives," *IEEE Trans. Ind. Electron.*, vol. 65, no. 3, pp. 2049–2056, Mar. 2018.
- [17] X. Zhang, T. Zhao, W. Mao, D. Tan, and L. Chang, "Multilevel inverters for grid-connected photovoltaic applications: Examining emerging trends," *IEEE Power Electron. Mag.*, vol. 5, no. 4, pp. 32–41, Dec. 2018.
- [18] B. Xiao, L. Hang, J. Mei, C. Riley, L. M. Tolbert, and B. Ozpineci, "Modular cascaded H-bridge multilevel PV inverter with distributed MPPT for grid-connected applications," *IEEE Trans. Ind. Appl.*, vol. 51, no. 2, pp. 1722–1731, Mar./Apr. 2015.
- [19] S. Daher, J. Schmid, and F. L. M. Antunes, "Multilevel inverter topologies for stand-alone PV systems," *IEEE Trans. Ind. Electron.*, vol. 55, no. 7, pp. 2703–2712, Jul. 2008.
- [20] J.-J. Jung, S. Cui, J.-H. Lee, and S.-K. Sul, "A new topology of multilevel VSC converter for a hybrid HVDC transmission system," *IEEE Trans. Power Electron.*, vol. 32, no. 6, pp. 4199–4209, Jun. 2017.
- [21] M. B. Ghat and A. Shukla, "A new H-bridge hybrid modular converter (HBHMC) for HVDC application: Operating modes, control, and voltage balancing," *IEEE Trans. Pow. Electron.*, vol. 33, no. 8, pp. 6537–6554, Sep. 2018.
- [22] A. Sinha, K. C. Jana, and M. K. Das, "An inclusive review on different multi-level inverter topologies, their modulation and control strategies for a grid connected photo-voltaic system," *Sol. Energy*, vol. 170, pp. 633–657, Aug. 2018.
- [23] H. Aburub, J. Holtz, and J. Rodriguez, "Medium-voltage multilevel converters-state of the art, challenges, and requirements in industrial applications," *IEEE Trans. Ind. Electron.*, vol. 57, no. 8, pp. 2581–2596, Aug. 2010, doi: 10.1109/TIE.2010.2043039.
- [24] A. Salem, H. Van Khang, K. G. Robbersmyr, M. Norambuena, and J. Rodriguez, "Voltage source multilevel inverters with reduced device count: Topological review and novel comparative factors," *IEEE Trans. Power Electron.*, vol. 36, no. 3, pp. 2720–2747, Mar. 2021, doi: 10.1109/TPEL.2020.3011908.
- [25] M. Sarebanzadeh, M. A. Hosseinzadeh, C. Garcia, E. Babaei, S. Islam, and J. Rodriguez, "Reduced switch multilevel inverter topologies for renewable energy sources," *IEEE Access*, vol. 9, pp. 120580–120595, 2021, doi: 10.1109/ACCESS.2021.3105832.
- [26] R. H. Baker and L. H. Bannister, "Electric power converter," U.S. Patent 3 867 643, Feb. 14, 1975.
- [27] R. H. Baker, "Switching circuit," U.S. Patent 4 210 826, Jul. 1, 1980.
- [28] A. Nabae, I. Takahashi, and H. Akagi, "A new neutral-point-clamped PWM inverter," *IEEE Trans. Ind. Appl.*, vol. IA-17, no. 5, pp. 518–523, Sep. 1981.
- [29] A. Nabae, I. Takahashi, and H. Akagi, "A neutral-point-clamped PWM inverter," in *Proc. Conf. Rec. IEEE IAS Annu. Meeting*, Cincinnati, OH, USA, Sep. 1980, pp. 761–766.
- [30] Z. Cheng and B. Wu, "A novel switching sequence design for five-level NPC/H-bridge inverters with improved output voltage spectrum and minimized device switching frequency," *IEEE Trans. Power Electron.*, vol. 22, no. 6, pp. 2138–2145, Nov. 2007.
- [31] I. Etxeberria-Otadui, A. L. de Heredia, J. San-Sebastian, H. Gaztaaga, U. Viscarret, and M. Caballero, "Analysis of a H-NPC topology for an AC traction front-end converter," in *Proc. 13th EPE-PEMC*, Sep. 2008, pp. 1555–1561.
- [32] V. Guennegues, B. Gollentz, L. Leclere, F. Meibody-Tabar, and S. Rael, "Selective harmonic elimination PWM applied to H-bridge topology in high speed applications," in *Proc. Int. Conf. Power Eng., Energy Electr. Drives*, Mar. 2009, pp. 152–156.
- [33] F. Kieferndorf, M. Basler, L. A. Serpa, J.-H. Fabian, A. Coccia, and G. A. Scheuer, "A new medium voltage drive system based on ANPC-5L technology," in *Proc. IEEE Int. Conf. Ind. Technol.*, Viña del Mar, Chile, Mar. 2010, pp. 605–611.
- [34] T. Chaudhuri, P. Steimer, and A. Rufer, "Introducing the common cross connected stage (C³S) for the 5L ANPC multilevel inverter," in *Proc. IEEE Power Electron. Specialists Conf.*, Jun. 2008, pp. 167–173.
- [35] P. K. Steimer, B. Odegard, O. Apeldoorn, S. Bernet, and T. Bruckner, "Very high power IGCT PEBB technology," in *Proc. IEEE 36th Power Electron. Specialists Conf.*, Jun. 2005, pp. 1–7.
- [36] P. Barbosa, P. Steimer, L. Meysenc, M. Winkelkemper, J. Steinke, and N. Celanovic, "Active neutral-point-clamped multilevel converters," in *Proc. IEEE 36th Conf. Power Electron. Spec.*, Jun. 16, 2005, pp. 2296–2301.
- [37] T. A. Meynard and H. Foch, "Multi-level conversion: High voltage choppers and voltage-source inverters," in *Proc. Rec. 23rd Annu. IEEE Power Electron. Spec. Conf. (PESC)*, Jun. 1992, pp. 397–403.
- [38] J. P. Lavieville, P. Carrere, and T. Meynard, "Electronic circuit for converting electrical energy, and a power supply installation making use thereof," U.S. Patent 5 668 711, Sep. 1997.
- [39] ABB. Accessed: Aug. 2020. [Online]. Available: <https://www.abb.com>
- [40] SIEMENS. Accessed: Aug. 2020. [Online]. Available: <https://www.siemens.com>
- [41] TMEIC-GE. Accessed: Aug. 2020. [Online]. Available: <https://www.tmeic-ge.com>
- [42] Ansaldo Sistemi Industriali. Accessed: Aug. 2020. [Online]. Available: <https://www.asiansaldo.com>

- [43] Convertteam. Accessed: Aug. 2020. [Online]. Available: <https://www.convertteam.com>
- [44] Eaton. Accessed: Aug. 2020. [Online]. Available: <https://www.eaton.com>
- [45] Arrowspeed. Accessed: Aug. 2020. [Online]. Available: <https://www.arrowspeed.com>
- [46] Ingeteam. Accessed: Aug. 2020. [Online]. Available: <https://www.ingeteam.com>
- [47] WEG. Accessed: Aug. 2020. [Online]. Available: <https://www.weg.net>
- [48] Rongxin Power Electronic Co. (RXPE). Accessed: Aug. 2020. [Online]. Available: <https://www.rxpe.co.uk>
- [49] LS Industrial Systems. Accessed: Aug. 2020. [Online]. Available: <http://eng.lsis.biz/>
- [50] Yaskawa. Accessed: Aug. 2020. [Online]. Available: <https://www.yaskawa.eu.com>
- [51] Beijing Leader & Harvest Electric Technologies. Accessed: Aug. 2020. [Online]. Available: <https://www.ld-harvest.com>
- [52] Schneider-Electric. Accessed: Aug. 2020. [Online]. Available: <https://www.schneider-electric.com>
- [53] Alstom. Accessed: Aug. 2020. [Online]. Available: <https://www.alstom.com>
- [54] Grupo Jema. Accessed: Aug. 2020. [Online]. Available: <https://www.grupojema.com>
- [55] PowerFlex 6000 Medium Voltage Drives Product Profile. Accessed: Aug. 2020. [Online]. Available: https://literature.rockwellautomation.com/idc/groups/literature/documents/pp/6000-pp003_-en-p.pdf
- [56] HIVECTOL—HVI—E Medium Voltage Multi-Level Drives Brochure. Accessed: Aug. 2020. [Online]. Available: https://www.hitachi.com.au/documents/product/Variable_Speed_Drives_Brochure.pdf
- [57] ABB General Purpose Drives ACS580MV Catalog. Accessed: Aug. 2020. [Online]. Available: https://library.e.abb.com/public/80d9e920d55846ad90bf2147fb7afaf/ACS580_catalog_3BHT490775R0001_RevC_EN.pdf
- [58] Siemens Prefect Harmony GH180. Accessed: Aug. 2020. [Online]. Available: <https://new.siemens.com/global/en/products/drives/sinamics/medium-voltageconverters/sinamics-perfect-harmony-gh180.html>
- [59] M. Vjeh, M. Rezanejad, E. Samadaei, and K. Bertilsson, "A general review of multilevel inverters based on main submodules: Structural point of view," *IEEE Trans. Power Electron.*, vol. 34, no. 10, pp. 9479–9502, Oct. 2019, doi: [10.1109/TPEL.2018.2890649](https://doi.org/10.1109/TPEL.2018.2890649).
- [60] B. Bugiardini and F. Jason, "Matching VFD to application requirements," Rockwell Automation on Demand Webinars, Jun. 2020. [Online]. Available: <https://www.rockwellautomation.com/en-us/company/events/webinars/on-demand.html>
- [61] M. M. Islam, M. A. G. Khan, M. A. Malek, and M. Y.-Y.-U. Haque, "Analysis of an IGBT based AC chopper driving RL load for oscillation free output voltage," in *Proc. 2nd Int. Conf. Robot., Electr. Signal Process. Techn. (ICREST)*, DHAKA, Bangladesh, Jan. 2021, pp. 95–99, doi: [10.1109/ICREST51555.2021.9331212](https://doi.org/10.1109/ICREST51555.2021.9331212).
- [62] M. Rastogi, R. H. Osman, and Y. Fukuta, "Variable-frequency drive with regeneration capability," U.S. Patent 7 508 147, Mar. Mar. 24, 2009.
- [63] J. Wang and Y. Li, "PWM rectifier in power cell of cascaded H-bridge multilevel converter," in *Proc. Int. Conf. Electr. Mach. Syst. (ICEMS)*, Seoul, South Korea, Oct. 2007, pp. 18–21.
- [64] M. A. Perez, J. R. Espinoza, J. R. Rodriguez, and P. Lezana, "Regenerative medium-voltage AC drive based on a multicell arrangement with reduced energy storage requirements," *IEEE Trans. Ind. Electron.*, vol. 52, no. 1, pp. 171–180, Feb. 2005, doi: [10.1109/TIE.2004.841095](https://doi.org/10.1109/TIE.2004.841095).
- [65] J. Rodriguez, L. Morán, J. Pontt, J. L. Hernández, L. Silva, C. Silva, and P. Lezana, "High-voltage multilevel converter with regeneration capability," *IEEE Trans. Ind. Electron.*, vol. 49, no. 4, pp. 839–846, Aug. 2002, doi: [10.1109/TIE.2002.801238](https://doi.org/10.1109/TIE.2002.801238).
- [66] P. Lezana, J. Rodriguez, D. Rojas, and J. Pontt, "Novel cell based on reduced single-phase active front end for multicell converters," in *Proc. 31st Annu. Conf. IEEE Ind. Electron. Soc. (IECON)*, Raleigh, NC, USA, Nov. 2005, p. 6, doi: [10.1109/IECON.2005.1568995](https://doi.org/10.1109/IECON.2005.1568995).
- [67] P. Lezana, J. Rodríguez, and D. A. Oyarzún, "Cascaded multilevel inverter with regeneration capability and reduced number of switches," *IEEE Trans. Ind. Electron.*, vol. 55, no. 3, pp. 1059–1066, Mar. 2008, doi: [10.1109/TIE.2008.917095](https://doi.org/10.1109/TIE.2008.917095).
- [68] J. Rodriguez, J. Pontt, E. Silva, J. Espinoza, and M. Perez, "Topologies for regenerative cascaded multilevel inverters," in *Proc. IEEE 34th Annu. Conf. Power Electron. Spec. (PESC)*, Acapulco, Mexico, Jun. 2003, pp. 519–524, doi: [10.1109/PESC.2003.1218109](https://doi.org/10.1109/PESC.2003.1218109).
- [69] J. R. Rodriguez, J. W. Dixon, J. R. Espinoza, J. Pontt, and P. Lezana, "PWM regenerative rectifiers: State of the art," *IEEE Trans. Ind. Electron.*, vol. 52, no. 1, pp. 5–22, Feb. 2005, doi: [10.1109/TIE.2004.841149](https://doi.org/10.1109/TIE.2004.841149).
- [70] S. Badawi, M. Narimani, Z. Cheng, and N. R. Zargari, "A new reduced switch-count configuration for regenerative cascaded H-bridge converter," in *Proc. IEEE Energy Convers. Congr. Expo. (ECCE)*, Detroit, MI, USA, Oct. 2020, pp. 4970–4975, doi: [10.1109/ECCE44975.2020.9235458](https://doi.org/10.1109/ECCE44975.2020.9235458).
- [71] S. Badawi, "A new switch-count reduction configuration and new control strategies for regenerative cascaded H-bridge medium voltage motor drives," M.S. thesis, McMaster Univ., Hamilton, ON, Canada, Oct. 2020.
- [72] S. Badawi, A. Abuelnaga, Z. Ni, S. Yuan, M. Narimani, Z. Cheng, and N. R. Zargari, "Utilization of a reduced switch-count topology in regenerative cascaded H-bridge (CHB) medium-voltage drives," *IEEE J. Emerg. Sel. Topics Power Electron.*, early access, Nov. 17, 2021, doi: [10.1109/JESTPE.2021.3129137](https://doi.org/10.1109/JESTPE.2021.3129137).
- [73] G.-T. Kim and T. A. Lipo, "VSI-PWM rectifier/inverter system with a reduced switch count," in *Proc. Conf. Rec. IEEE Ind. Appl. Conf. 30th IAS Annu. Meeting*, Orlando, FL, USA, Nov. 1995, pp. 2327–2332, doi: [10.1109/IAS.1995.530598](https://doi.org/10.1109/IAS.1995.530598).
- [74] A. Abuelnaga, M. Narimani, and A. S. Bahman, "A review on IGBT module failure modes and lifetime testing," *IEEE Access*, vol. 9, pp. 9643–9663, 2021, doi: [10.1109/ACCESS.2021.3049738](https://doi.org/10.1109/ACCESS.2021.3049738).
- [75] A. Abuelnaga, M. Narimani, and A. S. Bahman, "Power electronic converter reliability and prognosis review focusing on power switch module failures," *J. Power Electron.*, vol. 21, no. 6, pp. 865–880, Jun. 2021, doi: [10.1007/s43236-021-00228-6](https://doi.org/10.1007/s43236-021-00228-6).
- [76] B. J. Baliga, *The IGBT Device: Physics, Design and Applications of the Insulated Gate Bipolar Transistor*. Amsterdam, The Netherlands: Elsevier, 2015.
- [77] Z. Ni, A. Abuelnaga, M. Narimani, and N. R. Zargari, "DC-link voltage ripple control of regenerative CHB drives for capacitance reduction," *IEEE Trans. Ind. Electron.*, vol. 69, no. 4, pp. 3245–3254, Apr. 2022, doi: [10.1109/TIE.2021.3076727](https://doi.org/10.1109/TIE.2021.3076727).
- [78] K. Ravinchandra, T. K. S. Freddy, J. S. Lee, K. B. Lee, H. A. Mantooth, V. Thiruchelvam, and J. I. Y. Y. Xian, "Review of wide band-gap technology: Power device, gate driver, and converter design," *J. Power Electron.*, vol. 22, pp. 1–16, Jun. 2022.



DOHO KANG received the B.E. degree in electrical and computer engineering and the M.A.Sc. degree in electrical engineering specializing in power engineering from McMaster University, Hamilton, ON, Canada, in 2019 and 2022, respectively. He is currently an Hardware Development Engineer with Rockwell Automation Inc., Cambridge, ON, Canada.



SARAH BADAWI (Graduate Student Member, IEEE) received the B.Sc. degree (Hons.) in electrical engineering from Ain Shams University, Cairo, Egypt, in 2016, and the M.Sc. degree from McMaster University, Hamilton, Canada, in 2020, where she is currently pursuing the Ph.D. degree with the Electrical and Computer Engineering Department. Since September 2018, she has been a Research Assistant with the High Power Electronics Laboratory (HiPEL), McMaster University, and has been working in collaboration with the Research and Development in Rockwell Automation Inc., Cambridge, ON, Canada to develop new generations of motor drives. Her research interests include solid state transformers, EV extreme fast charging systems, grid-connected systems, high-power multilevel inverters, motor drives, and power electronics converters control.



ZHITUO NI (Member, IEEE) received the Ph.D. degree in electrical engineering from McMaster University, Hamilton, ON, Canada, in 2021. He is currently a Power Electronics Engineer with Rockwell Automation Inc., Cambridge, ON, Canada. His current research interests include power conversion and advanced control of grid-tied high-power converters.



MEHDI NARIMANI (Senior Member, IEEE) received the Ph.D. degree in electrical engineering from the University of Western Ontario, London, ON, Canada, in 2012. He was a Power Electronics Engineer at Rockwell Automation Inc., Cambridge, ON, Canada. He is currently an Associate Professor with the Department of Electrical and Computer Engineering, McMaster University, Hamilton, ON, Canada. He also holds the NSERC Canada Research Chair (CRC) position in high power converter systems. He has authored/coauthored more than 140 journals and conference proceeding papers, coauthored a Wiley-IEEE Press book, and holds seven issued/pending U.S./European patents. His current research interests include power conversion, high-power converters, control of power electronics converters, fast EV chargers, and wireless EV charging systems.



AHMED H. ABUELNAGA (Member, IEEE) received the B.Sc. (Hons.) and M.Sc. degrees from Ain Shams University, Cairo, Egypt, in 2012 and 2017, respectively, and the Ph.D. degree from McMaster University, Hamilton, ON, Canada, in 2021. From 2012 to 2017, he was a Teaching Staff at the Department of Electrical Power and Machines, Ain Shams University. From 2018 to 2021, he was in collaboration with Research and Development at Rockwell Automation Inc., Cambridge, ON, Canada. He is currently a Control Firmware Engineer with Rockwell Automation Inc., Cambridge. His research interests include power electronics interfaces, motor drives, embedded control, reliability, and predictive maintenance.



DAVID R. ZARGARI (Fellow, IEEE) received the B.Eng. degree from Tehran University, Iran, in 1987, and the M.A.Sc. and Ph.D. degrees from Concordia University, Montreal, QC, Canada, in 1991 and 1995, respectively.

He has been with Rockwell Automation Inc., Canada, since 1994, as a Senior Designer, a Researcher, and recently in a variety of Research and Development leadership roles. For the past 25 years he has been involved with design of power converters for AC drives. He has coauthored more than 100 research papers and two books, *Power Conversion and Control of Wind Energy Systems* and *Modular Multilevel Converters: Analysis, Control and Applications*. He holds more than 40 granted/pending patents in areas of power converters and medium voltage applications. His research interests include power converter topologies and their control aspects, power semiconductors, and renewable energy sources.

Dr. Zargari is registered as a Professional Engineer in the Province of Ontario and was a recipient of the Premier's Innovation Award for the Innovator of the year from the Province of Ontario in 2009.

...